THE JOURNAL OF BIOLOGICAL CHEMISTRY VOL. 290, NO. 22, pp. 13840–13861, May 29, 2015

The Human Mitochondrial DNA Depletion Syndrome Gene *MPV17* Encodes a Non-selective Channel That Modulates Membrane Potential*

Received for publication, October 3, 2014, and in revised form, April 9, 2015 Published, JBC Papers in Press, April 10, 2015, DOI 10.1074/jbc.M114.608083

Vasily D. Antonenkov[‡1,2], **Antti Isomursu**[‡1], **Daniela Mennerich**[‡], **Miia H. Vapola**[‡], **Hans Weiher**[§], **Thomas Kietzmann**[‡], **and J. Kalervo Hiltunen**[‡3]

From the [‡]*Faculty of Biochemistry and Molecular Medicine, Biocenter Oulu, University of Oulu, P.O. Box 3000, FI-90014 Oulu, Finland and the* [§]*Heinrich Pette Institute, Leibniz Institute for Experimental Virology, 20251 Hamburg, Germany*

Background: MPV17 is a mitochondrial inner membrane protein with unknown function.
Results: Recombinant human MPV17 shows highly regulated channel-forming activity; the mitochondrial membrane potential and the reactive oxygen species formation were elevated in embryonic fibroblasts from *Mpv17*$^{-/-}$ mice.
Conclusion: MPV17 functions as a non-selective channel modulating the membrane potential to preserve mitochondrial homeostasis.
Significance: Our data are important for understanding the role of MPV17 protein under physiological and pathological conditions.

The human *MPV17*-related mitochondrial DNA depletion syndrome is an inherited autosomal recessive disease caused by mutations in the inner mitochondrial membrane protein MPV17. Although more than 30 *MPV17* gene mutations were shown to be associated with mitochondrial DNA depletion syndrome, the function of MPV17 is still unknown. Mice deficient in *Mpv17* show signs of premature aging. In the present study, we used electrophysiological measurements with recombinant MPV17 to reveal that this protein forms a non-selective channel with a pore diameter of 1.8 nm and located the channel's selectivity filter. The channel was weakly cation-selective and showed several subconductance states. Voltage-dependent gating of the channel was regulated by redox conditions and pH and was affected also in mutants mimicking a phosphorylated state. Likewise, the mitochondrial membrane potential ($\Delta\psi_m$) and the cellular production of reactive oxygen species were higher in embryonic fibroblasts from *Mpv17*$^{-/-}$ mice. However, despite the elevated $\Delta\psi_m$, the Mpv17-deficient mitochondria showed signs of accelerated fission. Together, these observations uncover the role of MPV17 as a $\Delta\psi_m$-modulating channel that apparently contributes to mitochondrial homeostasis under different conditions.

MPV17-related hepatocerebral mitochondrial DNA (mtDNA)[4] depletion syndrome (MDDS), including Navajo neurohepatopathy, is an inherited autosomal recessive disease with the hallmark feature of a highly reduced mtDNA copy number in affected tissues (1–3). Clinically, this infantile onset disease is characterized by developmental delay, liver dysfunction, sensory and motor neuropathy, and other manifestations (1, 2). So far, more than 30 mutations of the nuclear encoded gene for the small (18-kDa) inner mitochondrial membrane protein MPV17 (4) have been described (5). In line with this, severe mtDNA depletion in the liver, brain, and skeletal muscle was also detected in *Mpv17*$^{-/-}$ mice (4, 6–8). Remarkably, these mice showed signs of premature aging: gray coat color early in adulthood, age-dependent glomerulosclerosis, sensorineural deafness (6–9), and cataract.[5] The recent findings where liver-specific expression of human MPV17 in *Mpv17*$^{-/-}$ mice restored mtDNA copy number and oxidative phosphorylation proficiency and prevented ketogenic diet-induced liver failure (10) underscore the link between MPV17 function and *MPV17*-related MDDS.

MPV17 belongs to a family of integral membrane proteins consisting of four members (PXMP2, MPV17, MP-L, and FKSG24 (MPV17L2)) in mammals and two members (Sym1 and Yor292) in yeast (Fig. 1*A*). Mouse Pxmp2 is an abundant peroxisomal protein acting as a non-selective channel transferring small solutes across the peroxisomal membrane (11, 12). The Pxmp2 channel (pore diameter 1.4 nm) showed weak cation selectivity and no voltage dependence at low holding potentials (11). In contrast to the peroxisomal localization of Pxmp2, the Mpv17, MP-L, and Mpv17L2 proteins were detected in the inner mitochondrial membrane (4, 9, 13, 14). Some observations indicate an involvement of the Mpv17 protein in modulation of reactive oxygen species (ROS) production (7, 9). However, the precise function of Mpv17 in mitochondria has not been established. Our recent observations with mouse Mpv17 (15) and the detection of the pore-forming activity of Sym1, the

* This work was supported by grants from the Academy of Finland, the Sigrid Juselius Foundation, and Biocenter Oulu.
[1] Both authors contributed equally to this work.
[2] To whom correspondence may be addressed. Tel.: 358-40-512-3964; Fax: 358-8-531-5037; E-mail: vasily.antonenkov@oulu.fi.
[3] To whom correspondence may be addressed. Tel.: 358-294-48-1151; Fax: 358-8-531-5037; E-mail: kalervo.hiltunen@oulu.fi.
[4] The abbreviations used are: mtDNA, mitochondrial DNA; MCR, multiple channel recording; MDDS, mitochondrial DNA depletion syndrome; SCA, single channel analysis; TMRE, tetramethylrhodamine ester; ROS, reactive oxygen species; FCCP, carbonyl cyanide *p*-trifluoromethoxyphenylhydrazone; DCF-DA, 2′,7′-dichlorofluorescein diacetate.

[5] V. D. Antonenkov and M. H. Vapola, unpublished observation.

yeast ortholog of MPV17 (16), suggested that human MPV17 may also have a role as a non-selective channel. These findings, however, appeared to be counterintuitive because the localization of open non-selective channels in the inner mitochondrial membrane would not favor the preservation of a high membrane potential ($\Delta\psi_m$) under physiological conditions. Therefore, we hypothesized that the channels should reside in the membrane mostly in a closed conformation. This would require that they possess gating properties that are under strict regulatory control. Indeed, the notion that the amino acid sequence of MPV17 (176 amino acids) contains four cysteine residues and three putative phosphorylation sites (Fig. 1*B*) implies that this protein may act as a redox- and ATP-sensitive channel. Considering these predictions, we focused on characterization of the channel-forming potential of human MPV17 (including its mutated forms) under different conditions that can be expected in mitochondria.

Predictably, opening of the non-selective channel in the inner mitochondrial membrane would lead to a decrease in $\Delta\psi_m$ that may be beneficial under some conditions to preserve mitochondrial homeostasis by preventing excessive production of ROS (17, 18). To prove this, we analyzed $\Delta\psi_m$ and ROS production in embryonic fibroblasts from *Mpv17*$^{-/-}$ mice. Moreover, we tried to outline the effects of Mpv17 deficiency on some $\Delta\psi_m$-dependent mitochondrial processes, such as the dynamics of these organelles and mitophagy.

We found that recombinant MPV17 forms a non-selective channel with gating properties affected by $\Delta\psi_m$, redox state, pH, and mutations mimicking protein phosphorylation. Embryonic fibroblasts from *Mpv17*$^{-/-}$ mice showed an abnormally high $\Delta\psi_m$ that was abrogated under conditions of chronic oxidative stress. Likewise, an increase in ROS production was registered in *Mpv17*$^{-/-}$ fibroblasts. In addition, Mpv17-deficient mitochondria were prone to fission even at elevated $\Delta\psi_m$, and *Mpv17*$^{-/-}$ fibroblasts showed signs of compromised PINK1/Parkin-dependent mitophagy. Together, these observations uncover the channel function of MPV17 and point to the role of this channel as a modulator of $\Delta\psi_m$ to preserve mitochondrial homeostasis.

Experimental Procedures

Yeast Strain and Growth Media—The *Pichia pastoris* strain SMD1163 (pep4, prb1, his4) was used for expression of human MPV17. For cell propagation and expression of recombinant protein, the standard BMGY and BMMY media were used. BMGY medium contained 1.0% (w/v) yeast extract, 2.0% (w/v) peptone, 1.34% (w/v) yeast nitrogen base (w/v), 1.0% (v/v) glycerol, and 4×10^{-5}% (w/v) biotin in 100 mM potassium phosphate buffer, pH 6.0. BMMY medium contained 0.5% (v/v) methanol instead of glycerol.

Plasmids and Cloning Strategies—The construct for expression of human MPV17 contained an N-terminal decahistidyl (His_{10}) tag followed by a protease Xa cleavage site fused to the *MPV17*-coding region. The sequence preceding the *MPV17*-coding region was 5′-ATG GGC CAT CAT CAT CAT CAT CAT CAT CAT CAT CAT CAC AGC AGC GGC CAT ATC GAA GGT CGT CAT ATG CTC GAG-3′. The construct was obtained from Genscript and cloned as an EcoRI-KpnI fragment into the yeast expression vector pPICZA (Invitrogen) harboring the methanol-inducible promoter AOX1 (pPICZA-Xa-rMPV17). The resulting construct was linearized using SacI and transformed into *P. pastoris* cells by electroporation. Positive transformants were spotted using Zeocin in-plate medium (Invitrogen). Amino acid substitutions in MPV17 were generated using the QuikChange mutagenesis kit (Stratagene) and pPICZA-Xa-rMPV17 as a template. Primers used for mutations were as follows: p.D92K, 5′-GCA CTG AAG AAG ATG TTG TTG AAG CAG GGG GGC TTT GC-3′ (forward) and 5′-GCA AAG CCC CCC TGC TTC AAC AAC ATC TTC TTC AGT GC-3′ (reverse); p.P98L, 5′-TCA GGG GGG CTT TGC CTT GTG TTT TCT AGG CTG C-3′ (forward) and 5′-GCA GCC TAG AAA ACA CAA GGC AAA GCC CCC CTG A-3′ (reverse); p.T80A, 5′-TCG GTT CAT CCC TGG CGC TAC CAA AGT GGA TGC AC-3′ (forward) and 5′-GTG CAT CCA CTT TGG TAG CGC CAG GGA TGA ACC GA-3′ (reverse); p.T80D, 5′-ATC GGT TCA TCC CTG GCG ACA CCA AAG TGG ATG CAC-3′ (forward) and 5′-GTG CAT CCA CTT TGG TGT CGC CAG GGA TGA ACC GAT-3′ (reverse); p.C99A, 5′- GGG GGC TTT GCC CCG GCT TTT CTA GGC TGC TT-3′ (forward) and 5′- AAG CAG CCT AGA AAA GCC GGG GCA AAG CCC CC-3′ (reverse). Mutations were confirmed by sequencing, and plasmids were transformed into *P. pastoris* cells.

In Silico Analysis—A routine BLAST search for homologous protein sequences was performed on the ExPASy server. Multiple sequence alignments of protein sequences were done using the ClustalW program. The phylogenic tree was constructed exploiting the Phylogeny.Fr. To analyze the secondary structure of MPV17, we applied prediction programs available on the ExPASy server: PROF, GORIV, Jpred3, and APSSP. These methods are based on different algorithms that resulted in variations in the predictions. Therefore, the α-helices predicted by at least three of the four applied programs and long enough to penetrate the membrane lipid bilayer (18 amino acids) were selected for further analysis. The HMMTOP program was applied for prediction of transmembrane segments. The helical wheel representations of the chosen MPV17 α-helical segments were constructed using Java Applet. Protein phosphorylation sites were predicted using the NetPhos 2.0 server.

SDS-PAGE and Western Blotting—SDS-PAGE was carried out using 10% (w/v) polyacrylamide gels according to a standard procedure. Gels were stained with silver or Coomassie Brilliant Blue R-350 (Coomassie). Purified MPV17 was quantified by SDS-PAGE, comparing the intensity of Coomassie staining against a standard of known concentration (bovine serum albumin) determined by Bradford analysis (Bio-Rad). Immunoblotting based on the detection of His tag sequence was used to identify expression of recombinant protein and estimate yields of it during solubilization from membranes and purification procedure. Proteins were transferred from gels to a nitrocellulose membrane by semidry blotting (Bio-Rad), and immunodetection was performed using monoclonal anti-His tag antibodies (Qiagen). Anti-mouse IgG coupled with alkaline-phosphatase was used as the secondary antibody, and protein bands were visualized using a standard color development procedure. Primary antibodies against PINK1 protein (PINK1,

sc-33796), succinate dehydrogenase (SDHB, sc-25851), voltage-dependent anion channel (VDAC1, sc-390996), and subunit of mitochondrial ATPase (ATP5F1, sc-162553) were from Santa Cruz Biotechnology, Inc. Light chain 3 (LC3B) antibody was from Cell Signaling, and α-tubulin clone B-5-1-2 mouse monoclonal antibody was from Sigma-Aldrich. Protein bands were detected using the ECL chemiluminescence kit (Amersham Biosciences).

Expression and Purification of Recombinant MPV17 Protein—A single colony of *P. pastoris* harboring pPICZA-XarMPV17 was grown overnight at +30 °C in 2.0 ml of BMGY medium. The resulting culture was inoculated to 50 ml of the same medium, and the cultivation was repeated. After sedimentation, cells were suspended to $A_{600} = 1.0$ unit in 400 ml of BMMY medium and cultivated at 30 °C for 24 h. Cells were harvested by centrifugation and suspended in the "breaking" buffer: 50 mM potassium phosphate, pH 7.4, 5.0% (v/v) glycerol, complete mix of protease inhibitors (Roche Applied Science), and 1.0 mM PMSF. After a 30-min incubation on ice, cells were mechanically disrupted by glass beads using a FastPrep-24 device (MP Biomedicals). The resulting mesh was centrifuged at low (1500 × *g* for 10 min) and then at high (100,000 × *g* for 90 min) speeds to sediment cell debris and membrane fragments, respectively. The membrane pellet was suspended in the "lysis" buffer: 20 mM potassium phosphate, pH 7.4, 10% (v/v) glycerol, 2.0% (w/v) Fos-choline-12 (Anatrace), complete mix of protease inhibitors, and 1.0 mM PMSF. Solubilization of membrane proteins was carried out at +4 °C and constant mixing for 6.0 h. The insoluble material was removed by centrifugation, and the resulting supernatant was diluted (1:4) with the "binding" buffer: 50 mM potassium phosphate, pH 8.0, 500 mM NaCl, 30 mM imidazole, and 10% (v/v) glycerol. The final sample (about 200 ml) was mixed with washed nickel-nitrilotriacetic acid superflow resin (~400 mg; Qiagen) and incubated at +4 °C with rotation for 1.0 h to accomplish binding of recombinant MPV17 protein to the matrix. Then the matrix was packed into a Polyprep chromatography column (Bio-Rad) and treated with "washing" buffer: 50 mM sodium phosphate, pH 8.0, 500 mM NaCl, 100 mM imidazole, 10% (v/v) glycerol, and 0.5% (w/v) Fos-choline-12 until the removal of nearly all non-bound proteins, which was monitored by the UV_{280} absorbance measurement. Bound proteins were eluted using buffer containing 50 mM sodium phosphate, pH 7.4, 100 mM NaCl, 500 mM imidazole, and 0.25% (w/v) Fos-choline-12. Fractions enriched with MPV17 were combined, concentrated, and, after overnight dialysis against 50 mM sodium phosphate buffer (pH 7.4) containing 100 mM NaCl, 5.0% (v/v) glycerol, and 0.25% (w/v) Fos-choline-12, were subjected to size exclusion chromatography using a Superdex200-10/300 GL column (GE Healthcare) equilibrated with the same buffer. The isolated protein was concentrated and dialyzed against 10 mM Tris-Cl (pH 7.2) buffer containing 5.0% (v/v) glycerol and 0.25% (w/v) Fos-choline-12. The same isolation procedure was applied for purification of mutated MPV17 proteins. In some experiments, all media used for isolation of MPV17 protein contained 5 mM dithiothreitol (DTT) or 1.0 mM EGTA.

Mass Spectrometry and Circular Dichroism (CD) Analysis—The authenticity of purified recombinant MPV17 was verified using matrix-assisted laser desorption ionization time-of-light (MALDI-TOF) mass spectrometric analysis. The samples of isolated protein were subjected to SDS-PAGE, and the gel was stained with Coomassie Blue. The assumed MPV17 band was cut from the gel, and after elution, the sample was applied to a Voyager DE PRO spectrometer (Applied Biosystems). Circular dichroism spectra (190–250 nm) were recorded with a Jasco J-715 spectrometer (Jasco International) using a 2-mm quartz cuvette containing purified MPV17 (0.1 mg/ml) in 10 mM potassium phosphate (pH 6.8) and 0.1% (w/v) Fos-choline-10. Each recording was repeated at least four times.

Detection and Analysis of Channel-forming Activity—Electrophysiological parameters of the MPV17 channel were studied as described (11), using a Planar Lipid Bilayer Workstation equipped with a BC-535 amplifier and 8-pole low pass Bessel filter (Warner). Acquisition and analysis were done using the pCLAMP software (Axon). As an initial step in our electrophysiological study, we used multiple-channel recording (MCR) to register a large number of insertion events searching for optimal conditions for measurements, including electrolyte concentration and voltage dependence (19). In particular, MCR revealed stimulation of the insertion of MPV17 into an artificial membrane by 0.5% (w/v) non-ionic detergent Genapol X-080 (Fluka). This detergent was then used for dissolving of protein samples before registration of the activity. In depth analysis of the channel-forming activity was performed using single channel analysis (SCA), which allows characterization at high time resolution of a single channel molecule. All measurements were made in commercial chambers (Warner Instruments) with two (*cis*/*trans*) compartments (4.0 ml each) connected with a pair of Ag/AgCl electrodes via 3.0 M KCl-agar bridges and equipped with magnetic stirrers. Reported membrane potentials are referred to the *cis* compartment. Protein samples (2–3 μl) were added to the *trans* compartment. The data were filtered at 1.0 kHz and recorded at 2.0 kHz. Dependence of the MPV17 channel conductance on electrolyte concentration was measured as follows. After detection of a single channel insertion at symmetrical 2.0 M KCl as electrolyte (holding potential +10 mV), the bath solution was diluted to achieve the corresponding concentration of KCl. For detection of reversal potential, electrolyte gradients (1.0 M KCl *trans*/0.5 M KCl *cis* or 0.5 M $CaCl_2$ *trans*/0.15 M $CaCl_2$ *cis* compartment) were established after the formation of a stable lipid bilayer and insertion of a single channel. An estimation of the Ca^{2+}/Cl^- permeability ratio was done as described (20). For measurement of current-voltage relationships, the current was recorded after stepwise application of different holding potentials. Voltage-dependent gating was detected at different holding potentials by measuring mean current during a 60-s recording. The resulting data were then normalized to the maximal currents at the same holding potential calculated from the chord conductance (21). Open probability (P_{open}) is defined as the ratio of detected conductance to the conductance at the fully open state at the indicated holding potential. Hydrated radii of non-electrolytes that were used to estimate the size of the channel's pore by means of the polymer exclusion method were as follows: ethylene glycol, 0.26 nm;

glycerol, 0.31 nm; arabinose, 0.34 nm; PEG 200, 0.43 nm; PEG 300, 0.60 nm; PEG 400, 0.70 nm; PEG 600, 0.78 nm; PEG 1000, 0.94 nm; PEG 2000, 1.22 nm; PEG 3400, 1.63 nm. The measurements were made in symmetric 1.0 M KCl containing 20% (w/v) non-electrolyte and at a holding potential of +10 mV.

Genotyping—All animal care and handling procedures were approved by the National Animal Experiment Board of Finland. Detection of the wild-type and recombinant alleles of the mouse *Mpv17* gene was performed by PCR-based length polymorphism analysis on tail genomic DNA or on DNA isolated from embryonic fibroblasts using suitable primers: 1) Mpv wt/fw, 5′-CAG TAC ACT ACC TGC GGC TT-3′; 2) Mpv wt/rc, 5′-CTC TGA TGC TCA GAG GCC TG-3′; and 3) Mpv mut/rc, 5′-GGG TCA TTT CAG GTC CTT GG-3′. The recombinant allele corresponds to a PCR product of 459 bp, whereas the wild-type allele corresponds to a PCR product of 304 bp. The two bands were separated electrophoretically and visualized under a UV screen. Primary mouse embryonic fibroblasts (wild type and $Mpv17^{-/-}$) were prepared from individual embryonic day 13.5 embryos as described (6).

Mitochondrial Membrane Potential ($\Delta\psi_m$) Assay (Plate Reading)—Fibroblasts were cultured in complete Dulbecco´s modified Eagle's medium with 10% (w/v) fetal calf serum. Before measurements, cells were seeded on a 96-well plate at a density of 15,000 cells/well. After incubation in a humidified incubator with 5% (v/v) CO_2 at 37 °C for 24 h, cells were treated with 50 μM H_2O_2 for 4 h or with 200 μM H_2O_2 for 48 h. To reproduce chronic oxidative stress, fibroblasts were treated three times, every 5th day in a row, with 200 μM H_2O_2, and membrane potential was detected 48 h after the last injection. Control samples were incubated under the same conditions but without treatment with H_2O_2. After incubation, the cells were briefly washed with PBS and then stained with the fluorescent dye tetramethyl rhodamine ester (TMRE; 10, 20, or 30 nM; Abcam) for 30 min. The low concentrations of TMRE were chosen to prevent quenching of the dye (22). Where indicated, cells were treated with 20 μM FCCP (Abcam) for 10 min before staining with the dye. After incubation, cells were washed two times with 0.2% (w/v) BSA in PBS, and fluorescence was immediately measured in a plate reader at an excitation wavelength of 549 nm and an emission wavelength of 575 nm. In some experiments, the digital image analysis method (22, 23) was used to estimate $\Delta\psi_m$ in individual fibroblasts (see below). This approach allowed us to take variations in the electrochemical potential across cellular plasma membranes ($\Delta\psi_p$) (22) into consideration.

Detection of ROS Formation Using 2′,7′-Dichlorofluorescein Diacetate (DCF-DA)—Primary mouse embryonic fibroblasts ($Mpv17^{+/+}$ or $Mpv17^{-/-}$) were cultured as described above and were treated with the antioxidants: vitamin C (100 μM) or *N*-acetyl-L-cysteine (10 mM) for 2 h. Then the cells were stained with DCF-DA (10 μM) for 30 min. After incubation, the cells were washed two times with 0.2% (w/v) BSA in PBS, and fluorescence was immediately measured in a plate reader at an excitation wavelength of 488 nm and an emission wavelength of 530 nm (24, 25).

Fluorescence Microscopy—Fibroblasts were seeded on 35-mm μ-dishes at a density of 30000 cells per dish and were allowed to settle overnight. Where indicated, cells were treated with 20 μM FCCP for 10 min before staining with 30 or 200 nM TMRE for 30 min, washed briefly with PBS, and immediately imaged with an appropriate filter set for TMRE. For digital image analysis to estimate $\Delta\psi_m$ (see above), TMRE (30 nM) fluorescence intensities were detected from mitochondria-rich and -poor regions of individual fibroblasts (22, 23). Random images of cells were taken using an LSM700 microscope (Zeiss) and a ×40 objective (fluorescent excitation, 488 nm; emission, 575 nm). The fluorescence intensities were measured in pixels from square areas of ~1.0 μM^2. 8–10 measurements from the corresponding regions of the cells were randomly made using the same square area, and the results were averaged. The fluorescence ratios were then calculated by dividing the TMRE intensity of the mitochondria-rich region by that of the mitochondria-poor region of the fibroblasts. Altogether, about 60 cells were analyzed in each experimental group.

Analysis of Mitochondrial Morphology—Fibroblasts were stained with 200 nM TMRE and imaged as described above. Up to 200 cells were scored per experiment, and each experiment was done at least in triplicate. In a first approach, each cell was categorized into one of three groups: cells predominantly containing tubular, middle sized, or fragmented mitochondria. In a second set of experiments, the cells were classified according to length of mitochondria (26): elongated (at least 60% of mitochondria showing tubular structure over 2–3 μm), fragmented (no tubular structures over 2–3 μm), and intermediate structure of organelles. In both experimental settings, the analysis was done by an investigator blinded to the genotype and treatment of the cells.

Statistical Analysis—Data are presented as means ± S.D. If necessary, significance was determined using a two-tailed Student's *t* test.

Results

The sequence similarity between MPV17 and other members of the family, including Pxmp2, led to the hypothesis that all of these proteins form transmembrane channels. To support this, we first analyzed the amino acid sequence of MPV17 to reveal features characteristic for channel proteins. A hydropathy plot showed four potential membrane-spanning domains formed by hydrophobic and non-charged amino acids in MPV17 (1) (Fig. 1*B*). This prediction, however, may be misleading if one considers the overall structure of α-helical channels (17), which needs to fulfill certain thermodynamic requirements. In particular, the helices should contain hydrophilic amino acids along the side facing an interior of the channel's pore and hence show amphipathic properties (27, 28). In fact, by using algorithms predicting protein secondary structures (27), we identified five α-helical regions in the sequence of MPV17 that are long enough to penetrate a membrane lipid bilayer (minimum of 18 amino acids). Most of these α-helices are amphipathic, as revealed by helical wheel representations (Fig. 1*C*). Thus, these *in silico* analyses support our prediction that MPV17, like its peroxisomal counterpart Pxmp2, would be a channel-forming protein.

To show that MPV17 is indeed active as a channel, we expressed this protein with a His_{10} tag at its N terminus in yeast *P. pastoris* cells. The recombinant protein was isolated from the

crude membrane fraction using His tag affinity followed by size exclusion chromatography procedures. From a comparison with the retention time during size exclusion chromatography of soluble standard proteins, the molecular mass of MPV17 was estimated to be ~60 kDa (Fig. 2*A*), indicating that the protein is apparently a homotrimer. The protein migrated as a single band on SDS-PAGE, confirming that purification was near homogeneity (Fig. 2*B*). The authenticity of MPV17 was verified by mass spectrometry (data not shown). The absorbance curve of the CD spectrum (Fig. 2*C*) showed minima at 208 and 220 nm, indicating a preserved α-helical structure that corroborates our *in silico* analysis.

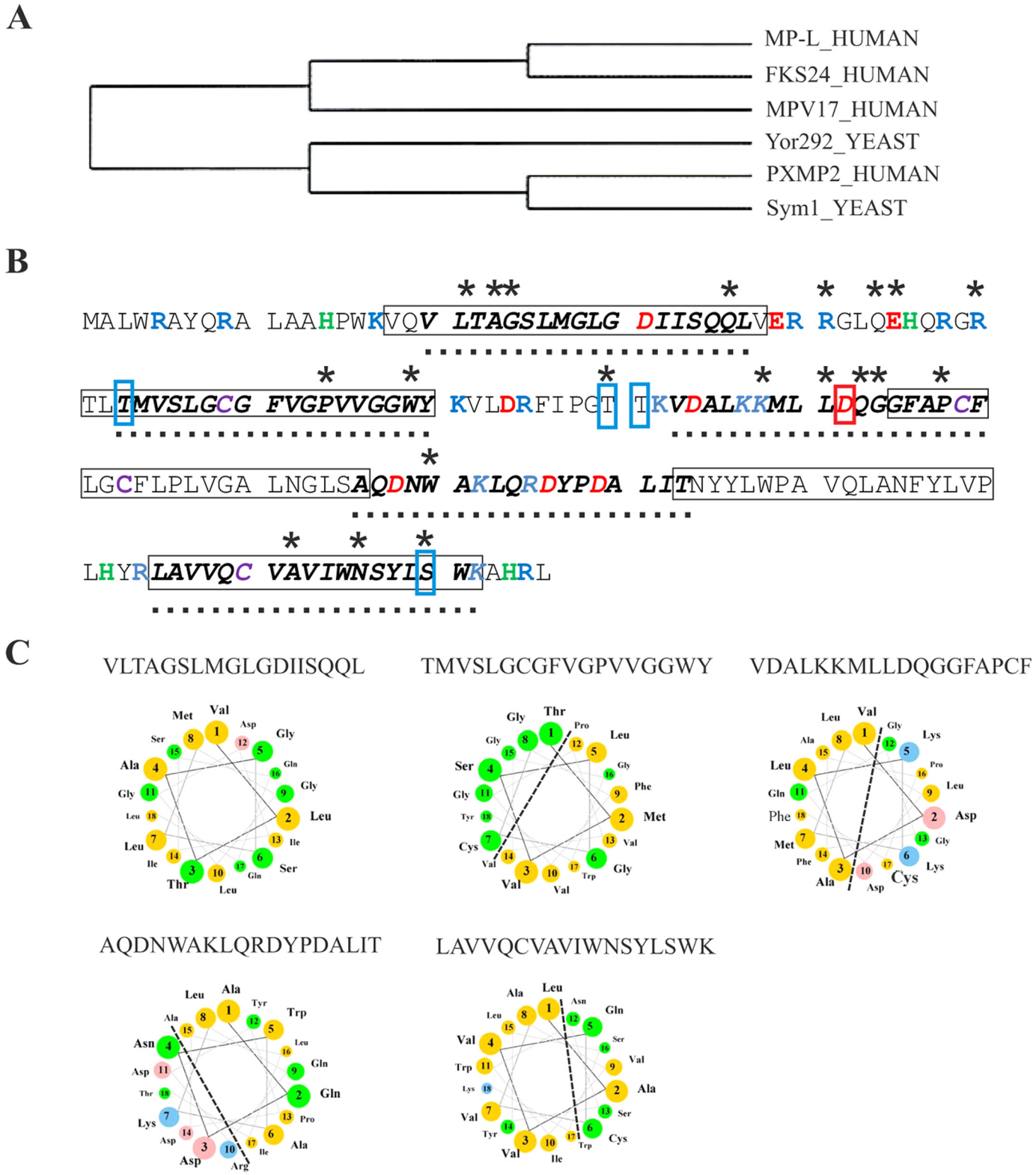

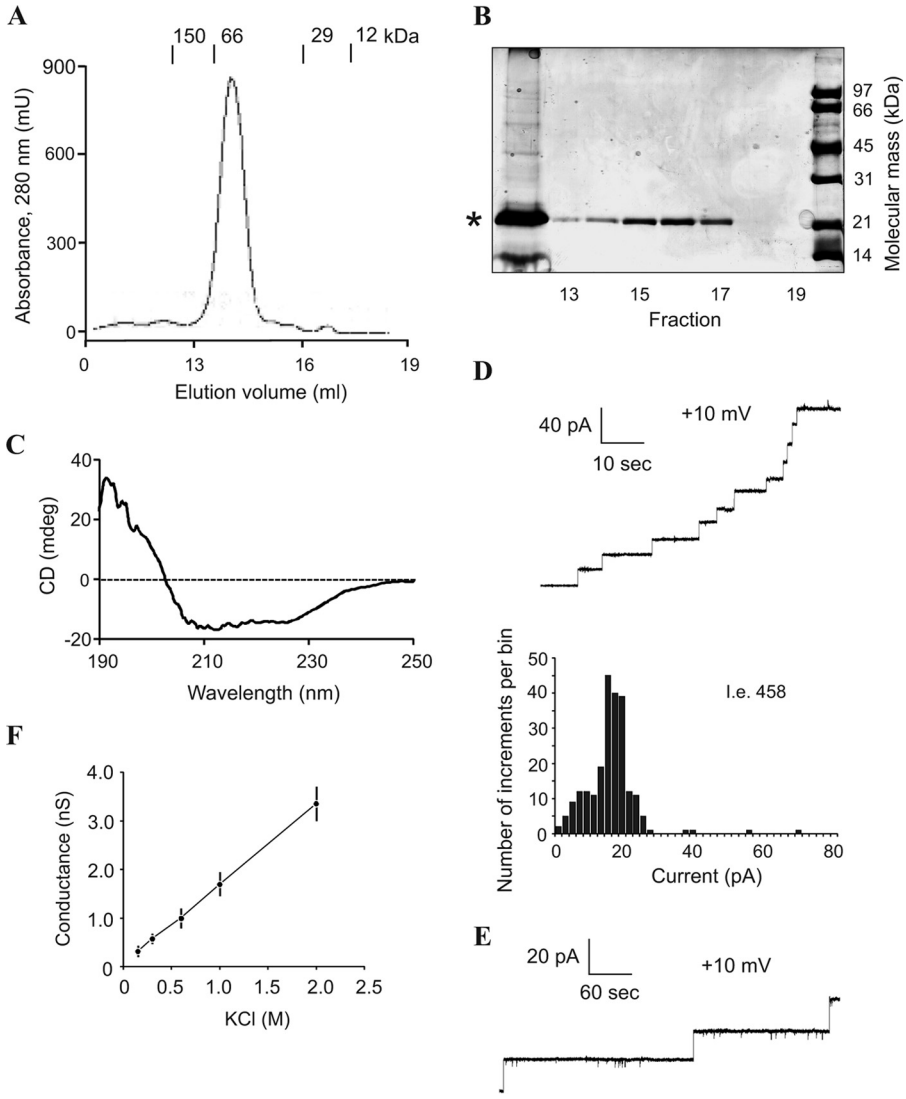

FIGURE 2. **Isolation of recombinant MPV17 protein and detection of channel-forming activity.** *A*, size exclusion chromatography of MPV17 after His tag affinity purification step. Positions of molecular mass markers are shown. *B*, Coommassie-stained SDS-PAGE of MPV17 samples obtained after His trap (*far left lane*) and size exclusion (*other lanes*) chromatography. The position of MPV17 is marked by an *asterisk*. *C*, secondary structure analysis of purified MPV17 using CD spectroscopy. *D*, MCR of isolated MPV17. *Top*, current trace of a membrane bilayer showing the insertion of multiple channels. Electrolyte was symmetrical 1.0 M KCl buffered with 10 mM Tris-Cl, pH 7.2. *Bottom*, histogram of the frequency of insertion events relative to their conductance. Bin size was 2 pA. The total number of calculated insertion events (*I.e.*) is indicated. *E*, long term recording of isolated MPV17 channel (see the legend to Fig. 2*D* for details). Note that the channels are permanently open for several min. *F*, single channel conductance of purified MPV17 as a function of KCl concentration ($n = 6$). *Error bars*, S.D.

Next, we studied the ability of the purified MPV17 to form channels in planar lipid bilayers. First, we conducted MCRs to optimize conditions for measurements. Insertion of MPV17 into an artificial membrane resulted in a stepwise increase in registered current (Fig. 2*D*, *top*), indeed reflecting the channel-forming activity of the protein. The histogram of insertion events (Fig. 2*D*, *bottom*) revealed one dominant peak of activity with an average current amplitude of 18–20 pA (symmetrical 1.0 M KCl, holding potential +10 mV). The channel tends to remain open at low membrane potentials for long periods of time (Fig. 2*E*). The conductance of the channel followed the electrolyte concentration (Fig. 2*F*). In a second set of experiments, we performed SCAs and showed that at moderate positive and negative membrane potentials, the MPV17 channel is

FIGURE 1. ***In silico* analysis of MPV17 sequence.** *A*, a phylogenic tree was constructed using amino acid sequences of human (PXMP2, MPV17, MP-L, and FKSG24/MPV17L2) and yeast *Saccharomyces cerevisiae* (Sym1 and Yor292) proteins that constitute the Pxmp2 family (see also Ref. 14). *B*, sequence of human MPV17 protein. Charged amino acids are *colored* as follows: Asp and Glu (*red*); Arg and Lys (*blue*); and His (*green*). The putative membrane-spanning domains predicted using the HMMTOP algorithm are shown in *boxes*. For the detection of putative α-helices, four different programs were used (see "Experimental Procedures" for details). The α-helices predicted by at least three of four applied programs and long enough to penetrate the membrane lipid bilayer (18 amino acids) were chosen for further analysis (marked in *boldface italic type* and *underlined*). Note that the putative membrane-spanning domains that are supposed to be α-helices (shown in *boxes*) do not necessarily coincide with the predicted α-helices (marked in *boldface italic type*). The locations of point mutations leading to MDDS are marked by *asterisks*. The aspartic acid (*D*) determining ion selectivity of the channel is marked by *red box*. The putative phosphorylation sites are shown by *blue boxes*. *C*, *helical wheel representations* of the sequences *underlined* in *B*. Amino acids are *colored* according to the physico-chemical properties of the side chains: hydrophobic (*yellow*); polar, uncharged (*green*); negatively charged (*pink*); and positively charged (*blue*). The sequences of the corresponding α-helices are shown *over* the *wheels*. *Dotted lines* separate mainly hydrophilic sides from mostly hydrophobic regions of the sequences.

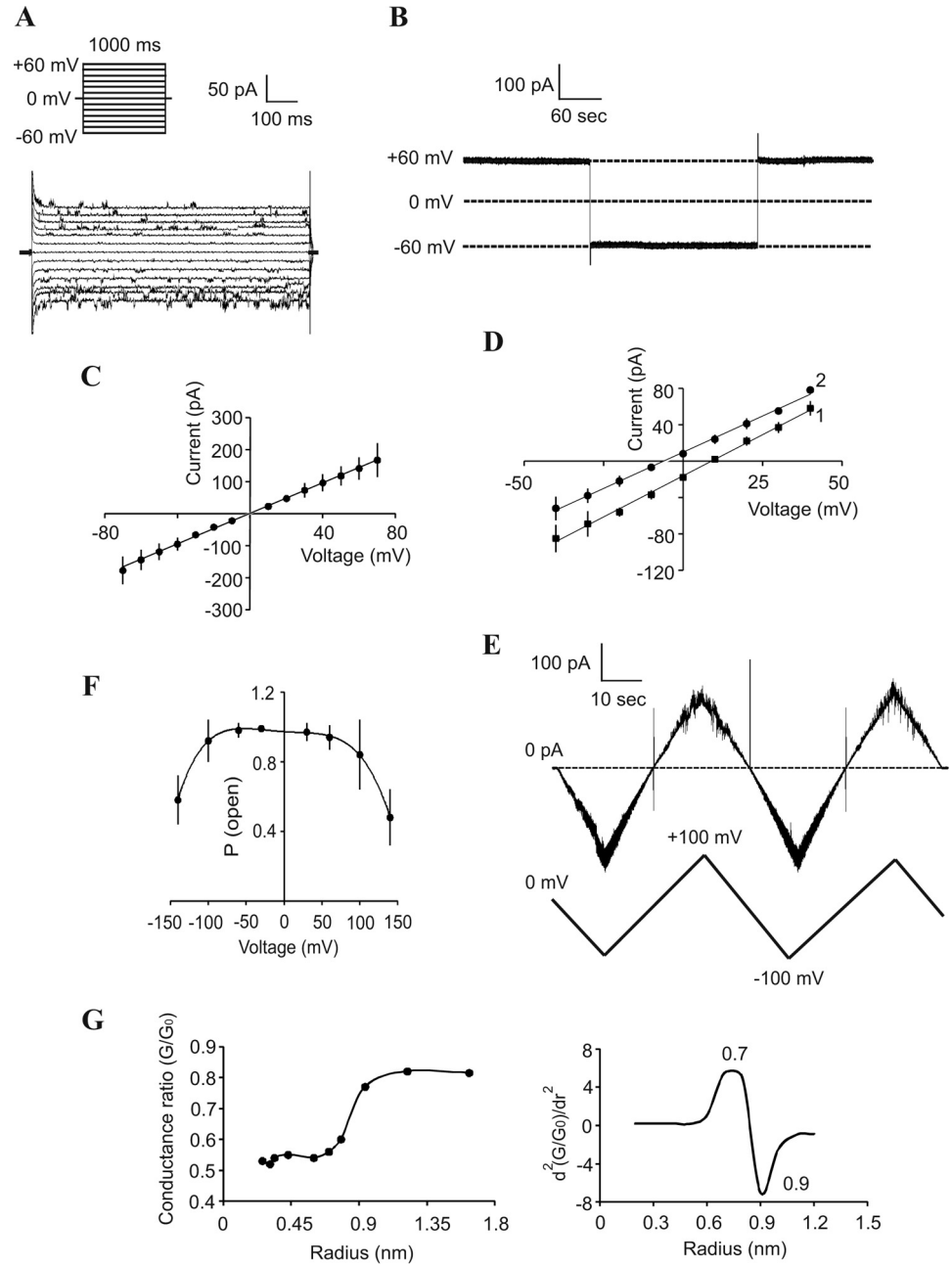

FIGURE 3. **SCA of isolated MPV17 protein.** *A*, recording of a single channel current using the indicated voltage-step protocol. Electrolyte (*A*, *B*, *C*, *E*, and *G*) was symmetrical 1.0 M KCl buffered with 10 mM Tris-Cl, pH 7.2. *B*, activity of a single channel was registered at moderate membrane potentials (±60 mV) and long term resolution. *C*, current-voltage relationship of a single MPV17 channel. *D*, current-voltage dependence of a single channel under asymmetric electrolyte conditions: 1.0 M KCl *trans*/0.5 M KCl *cis* (*1*) or 0.5 M $CaCl_2$ *trans*/0.15 M $CaCl_2$ *cis* (*2*). *E*, current trace of a single channel in response to the indicated voltage-ramping. *F*, voltage-dependent open probability (P_{open}) of the MPV17 channel. *G*, application of the polymer-exclusion method to estimate the size of the channel's pore. *Left*, 30–40 single insertion events registered without (G_0) or with (*G*) non-electrolyte by SCA were used to calculate the average conductance of the channel. The data are presented as ratio G/G_0 plotted against hydrated radii of non-electrolytes (see "Experimental Procedures" for details). *Right*, second derivative of the dependence from the *left panel*, indicating the maximal and the minimal turning points. The *upper point* (0.7 nm) predicts the molecular radius of solutes at which movement inside the pore becomes restricted. The *lower point* (0.9 nm) indicates the minimal radius of molecules that are not conducted by the channel. *Error bars*, S.D.

in an open conformation (Fig. 3*A*) that may last for a long period of time (Fig. 3*B*). Further, the channel showed a nearly linear current-voltage relationship with a slope conductance of $\Lambda = 2.2 \pm 0.3$ nanosiemens, $n = 10$ (symmetrical 1.0 M KCl, Fig. 3*C*). The reversal potentials of the channel in asymmetric (1.0 M KCl *trans*/0.5 M KCl *cis* or 0.5 M $CaCl_2$ *trans*/0.15 M $CaCl_2$ *cis*) solutions were $E_{rev} = +10.0$ mV and $E_{rev} = -5.6$ mV, respectively, indicating a P_{K+}/P_{Cl-} ratio of ~3.9 and a P_{Ca2+}/P_{Cl-} ratio of ~0.74 (Fig. 3*D*). An opposite ion selectivity of the MPV17 channel in $CaCl_2$ *versus* KCl solution is not surprising because the hydrated radius of the Ca^{2+} ion is significantly larger than that of the K^+ ion (29, 30). When measurements were made without reducing agents such as DTT, the channel was resistant to closing in the range of holding potentials of ±100 mV (Fig. 3, *E* and *F*). However, closing with an appearance of four main subconductance states was registered at hold-

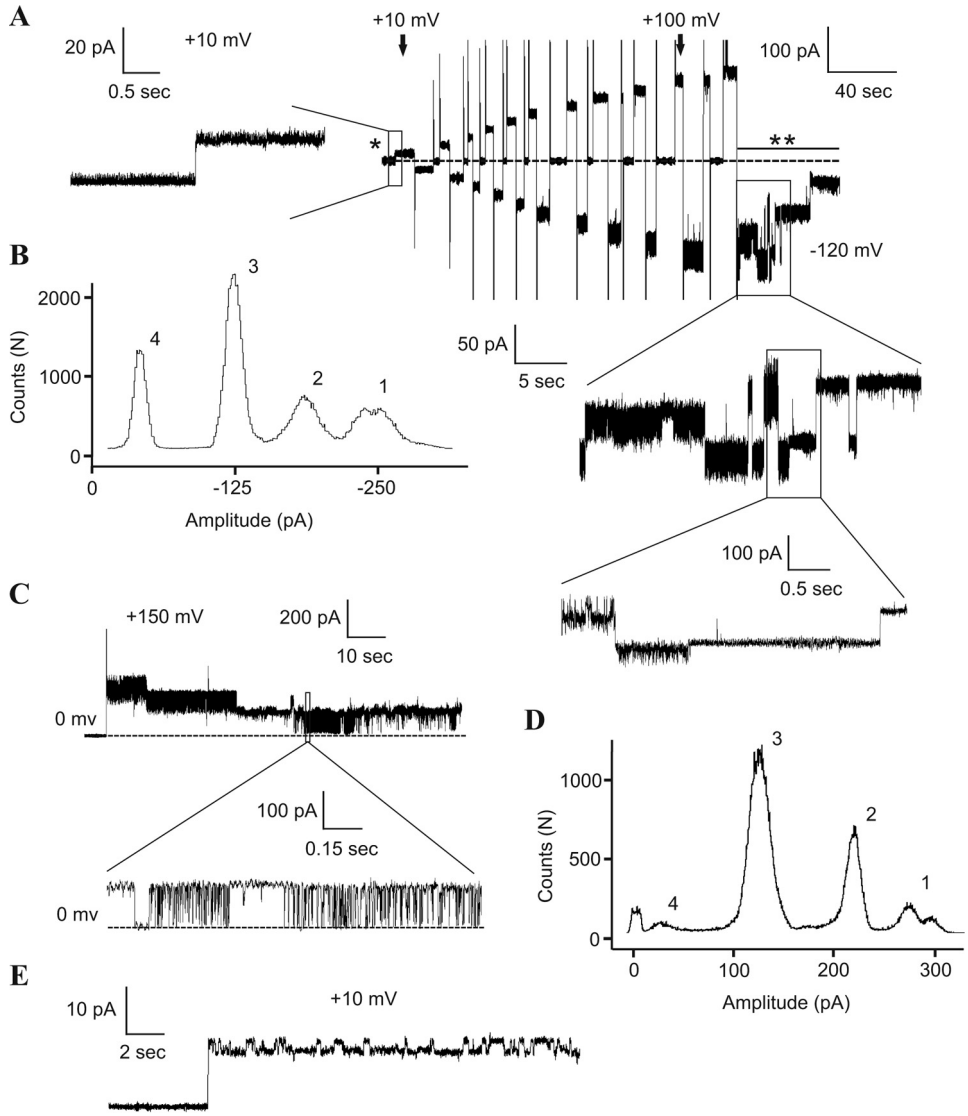

FIGURE 4. **Recordings of a single MPV17 channel at the different membrane potentials indicated.** The protein was isolated without DTT. *A*, current recording of a channel (insertion event is marked by a *single asterisk*) at successive step increases of positive and negative potentials. Electrolyte (*A*, *C*, and *E*) was symmetrical 1.0 M KCl (without DTT) buffered with 10 mM Tris-Cl, pH 7.2. Time scale-magnified traces of the insertion event (*left*) and channel closing (*below panels*) are shown. *B*, amplitude histogram derived from recording of the channel activity at −120 mV shown in *A* (the region of analysis is marked by a *heavy line* and *two asterisks*). Note several subconductance states of the channel, which are *numbered* starting from the fully open state. *C*, closing of a single MPV17 channel at +150 mV. A time scale-expanded trace is shown at the *bottom*. *D*, amplitude histogram of the recording shown in *C*. Note the similarity in the amplitudes derived at negative (*B*) and positive (*D*) membrane potentials and showing four subconductance states, where state 1 comprises two substates. *E*, insertion of a single channel (MCR) in a fully open conformation, indicating fluctuations of the current that apparently reflect transitions between two substates of the subconductance state 1 (see *B* and *D* for a comparison).

ing potentials from −100 to +100 mV (Fig. 4, *A*–*D*). Occasionally, small fluctuations of the current were registered on top of the fully open channel even at low membrane potentials (Fig. 4*E*). Incubation of protein samples with Ca^{2+} ($CaCl_2$; 20 μM or 0.1 mM), EGTA (0.1 mM or 1.0 mM), or P_i (potassium phosphate; 1.0 mM or 20 mM) did not affect the rate of insertion events, conductance, and gating properties of the MPV17 channel. Moreover, isolation of the Mpv17 protein in the presence of 1.0 mM EGTA to prevent interference by Ca^{2+} did not affect the channel-forming activity. We then used the polymer exclusion method in order to obtain information about the pore size of the channel and found that the diameter of the narrowest part of the pore (selectivity filter) is ~1.8 nm (Fig. 3*G*).

The presence of four cysteine residues within the MPV17 sequence implies redox sensitivity of the channel. Therefore, we used H_2O_2 and DTT as oxidizing and reducing agents, respectively, to test their effects on the properties of the MPV17 channel. Pretreatment of purified MPV17 with 0.2 mM H_2O_2 had no effect on the homotrimeric composition and the secondary structure of the protein (data not shown) and did not affect the slope conductance of the channel (Fig. 5*A*). However, the oxidative treatment increased the channel's resistance to voltage-dependent closing (Fig. 5, *A*–*C*). In contrast, incubation of the MPV17 protein with 10 mM DTT resulted in characteristic current-voltage dependence with current rectification, intensive flickering at negative holding potentials, and an evident tendency to close at positive voltages, although the channel's conductance was not affected (Fig. 5, *D* and *E*). The closing led frequently to the appearance of subconductance states (Fig. 5*E*). A quantitative estimation of

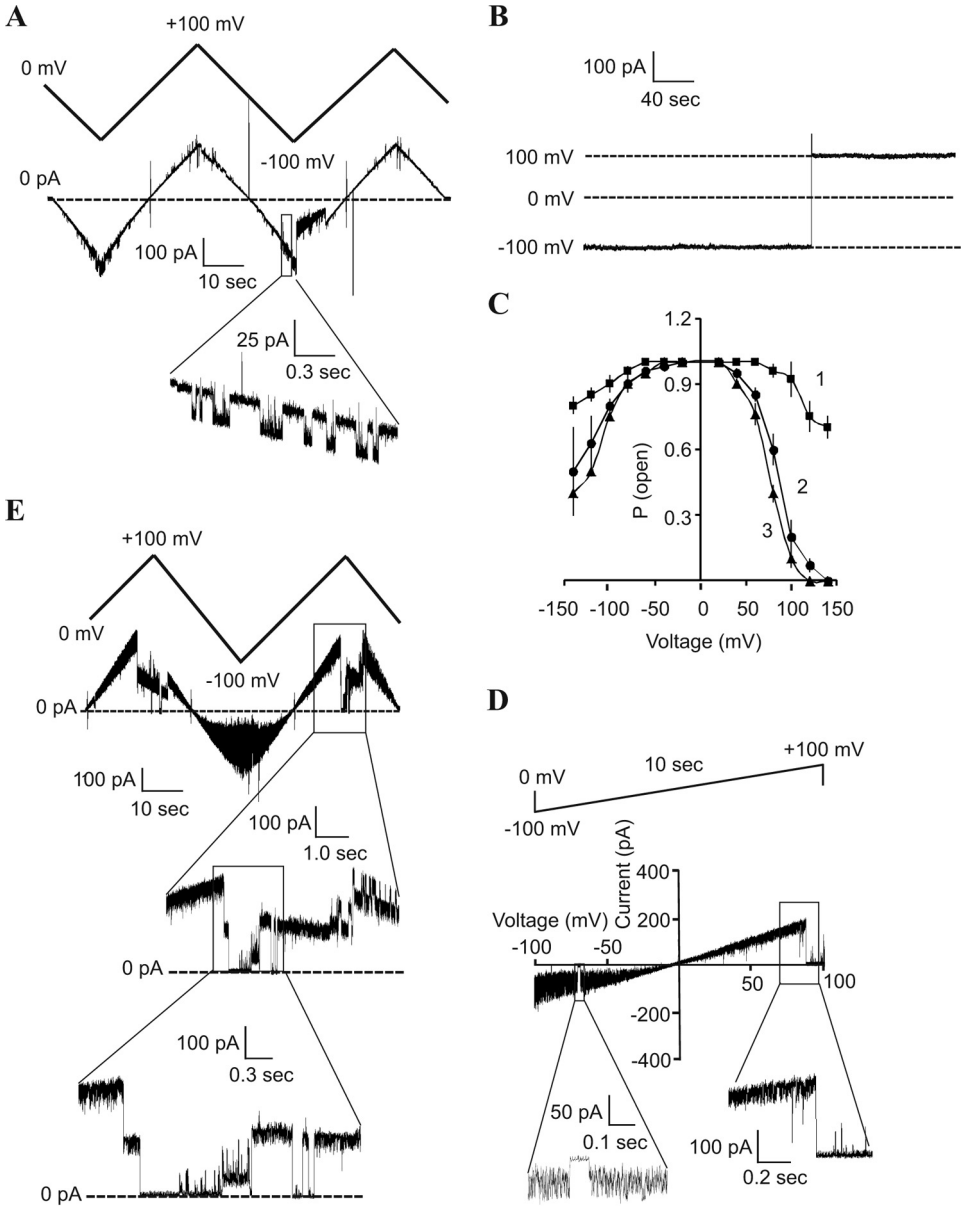

FIGURE 5. **Redox sensitivity of the purified MPV17 channel; effect of H_2O_2 and DTT.** *A*, MPV17 was isolated using a standard protocol and treated with 200 μM H_2O_2 for 30 min, and the peroxide was removed by dialysis. Shown is a current trace of a single channel in response to the indicated voltage ramp protocol. Electrolyte (*A–E*) was symmetrical 1.0 M KCl, pH 7.2. Note that H_2O_2 treatment did not affect conductance of the channel. The *bottom trace* represents time scale-expanded recording of the *top trace* and shows fluctuations of current amplitudes at the fully open state of the channel, which correspond to subconductance state 1 in Fig. 4, *B* and *D*. These fluctuations are characteristic for the channels pretreated with H_2O_2 and may cause some variations in conductance values obtained for the MPV17 channel at different conditions. *B*, current traces at a long term resolution indicating that at oxidative conditions (see above), the channel is in an open conformation even at elevated membrane potentials (±100 mV). *C*, voltage-dependent open probability (P_{open}) of MPV17 channel pretreated with 200 μM H_2O_2 (*1*) or 10 mM DTT (*2*) or isolated in the presence of 5 mM DTT (*3*); the measurements were made without (*1*) or with (*2* and *3*) 10 mM DTT ($n = 6–8$). *D*, current-voltage dependence of a single MPV17 channel preincubated with 10 mM DTT. Electrolyte (*D* and *E*) contained 10 mM DTT. The *bottom traces* represent time scale-expanded current recording of the *top trace*, indicating closing of the channel. *E*, current trace of two channels in response to the shown voltage ramping. MPV17 protein was isolated in the presence of 5 mM DTT. The *bottom traces* represent time scale-expanded recordings of the *top trace*, showing an appearance of subconductance states during closing of the channels. *Error bars*, S.D.

the open probability revealed that the channel is prone to closing under reducing conditions even at moderate holding potentials (Fig. 5*C*).

We next analyzed whether changes in pH affect the gating properties of the MPV17 channel under reducing conditions. A shift from the standard pH 7.2 to a more alkaline pH 8.2 did not affect conductance (data not shown) and voltage-dependent gating of the channel (Fig. 6, *A–C* and *E*). However, under mild acidic conditions (pH 5.8), the channel was more resistant to voltage-dependent closing (Fig. 6, *D* and *E*) with a tendency to show only partial closing at high holding potentials.

The most important functional part of any channel protein is the narrowest segment of the channel's pore, the so-called selectivity filter (29). It determines key parameters of a non-selective channel: the size exclusion limit as well as the ion selectivity. One way to reveal an amino acid sequence lining of the channel's pore is to detect amino acid(s) responsible for ion selectivity of this channel. As a rule, these amino acids are

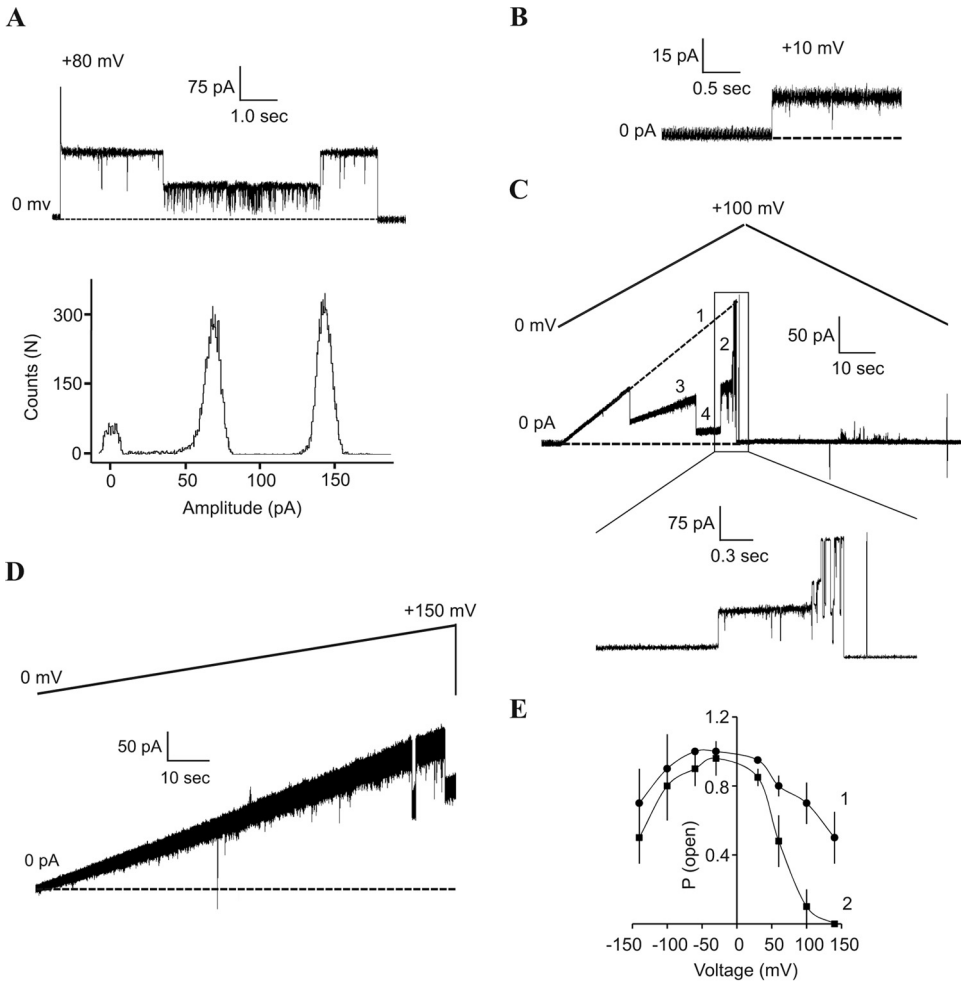

FIGURE 6. **Effect of pH on MPV17 channel activity when pretreated with DTT.** Electrolyte was symmetrical 1.0 M KCl containing 10 mM DTT and buffered with 10 mM Tris-Cl, pH 7.2 (*A*) and pH 8.2 (*B* and *C*), or with 10 mM sodium acetate, pH 5.8 (*D*). *A*, closing of a single channel at step increase of membrane potential to +80 mV (*top*). *Bottom*, amplitude histogram derived from the recording shown at the *top*. Note that the only two subconductance states were registered. *B*, insertion of a single channel at pH 8.2. *C*, current trace of a channel shown in *B* in response to the indicated voltage ramp protocol. The *bottom trace* represents a time scale-expanded recording of the *top trace*. All four subconductance states (*numbered*) were registered. *D*, current-voltage dependence of a single channel registered at pH 5.8. Note the partial closing of the channel at high membrane potential. *E*, voltage-dependent open probability (P_{open}) of the channel at pH 5.8 (*1*) or pH 8.2 (*2*) ($n = 4–6$). Electrolyte was symmetrical 1.0 M KCl containing 10 mM DTT and buffered with 10 mM sodium acetate (*1*) or 10 mM Tris-Cl (*2*). *Error bars*, S.D.

localized just in the selectivity filter or very close to it (17, 29). We noticed that the homologous proteins Pxmp2 (11), Sym1 (16), mouse Mpv17 (15), and human MPV17 (this study) are all cation-selective channels. The ion selectivity of these channels may be determined by the same conserved negatively charged amino acid(s). Given the role that MPV17 may play as a channel in the pathogenesis of MDDS, we considered that the selectivity filter might be formed by amino acids in the region showing a cluster of mutations causing MDDS (1, 5). Inspection of the MPV17 amino acid sequence revealed the conserved Asp-92 as a candidate amino acid determining cation selectivity of the channel (Fig. 1*B*). To test this, we introduced the point mutation p.D92K into MPV17 and analyzed its channel-forming activity (Fig. 7, *A–E*). The mutation did not significantly affect the slope conductance of the channel under symmetrical electrolyte conditions (Fig. 7*B*). This may indicate that Asp-92 is not just inside the selectivity filter but somewhere close to it. A certain spread of conductance values registered in our experiments, which apparently reflects the occurrence of two closely related substates of the MPV17 channel in the fully open conformation (e.g. see Fig. 4, *A–E*), did not allow us to make more precise comparisons between conductance data of the wild-type channel and its mutated variants. Likewise, we found a shift in the ion selectivity relative to the wild-type MPV17 channel: P_{K+}/P_{Cl-} ratio ~0.78 and $P_{Ca2+}/P_{Cl}-$ ratio ~0.45 (Fig. 7*C*), indicating that indeed Asp-92 is the ion selectivity-determining residue. Surprisingly, compared with the wild-type MPV17 protein, the mutant channel was less prone to voltage-dependent closing under reducing conditions (Fig. 7, *D* and *E*). The knowledge about the ion selectivity-determining residue allows us now to analyze the functional role of amino acid residues apparently contributing to formation of the channel's pore.

A dissipation of the mitochondrial membrane potential (*e.g.* using ionophores) does not cause membrane permeability for small solutes in the absence of specific physiological triggers (31) that contradicts the gating properties of the MPV17 channel (see above). Therefore, we hypothesized that in addition to the redox state and pH, other regulatory mechanisms may con-

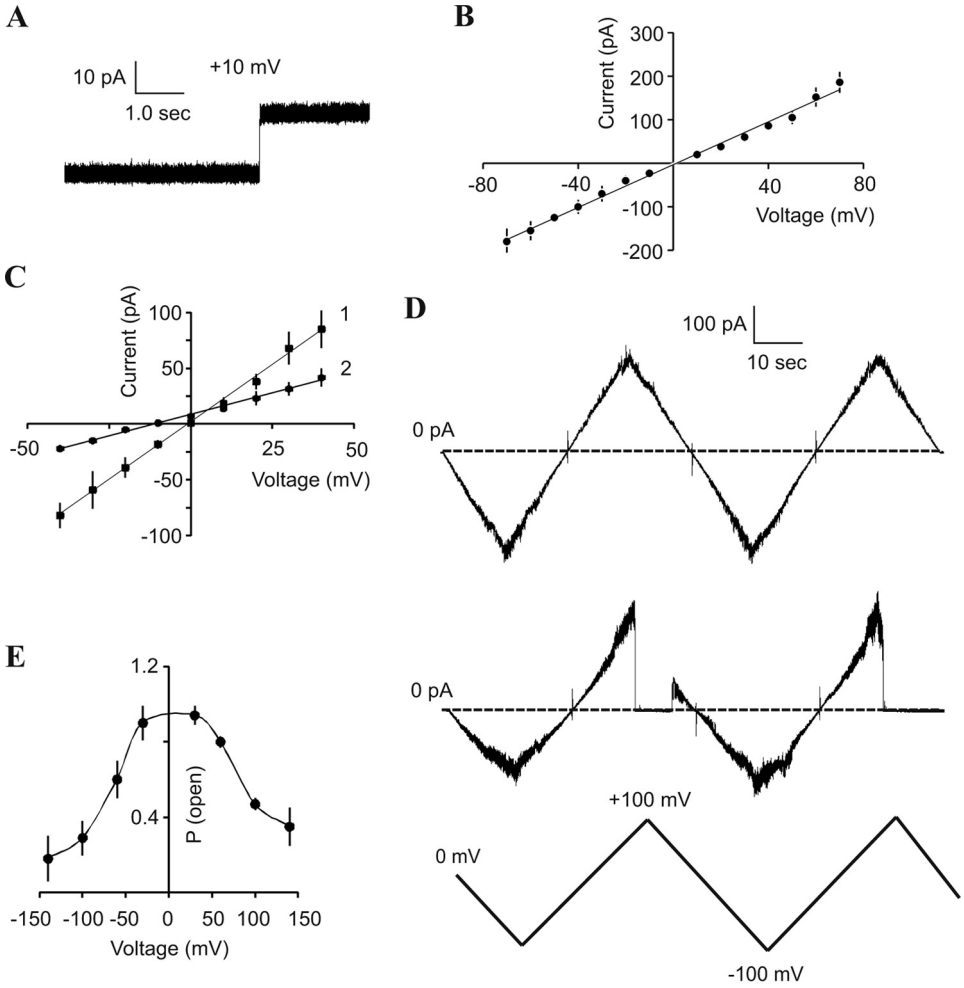

FIGURE 7. **SCA of MPV17 protein with mutation p.D92K.** *A*, current trace of a single channel. Electrolyte (*A*, *B*, and *D*) was symmetrical 1.0 M KCl, pH 7.2. *B*, current-voltage relationship of a mutant channel (electrolyte contained 10 mM DTT) ($n = 8–10$). *C*, current-voltage relationship of the channel under asymmetric electrolyte conditions: 1.0 M KCl *trans*/0.5 M KCl *cis* (*1*) or 0.5 M $CaCl_2$ *trans*/0.15 M $CaCl_2$ *cis* (*2*); all samples contained 10 mM DTT ($n = 8–10$). *D*, current trace of the channel in response to the indicated voltage ramp protocol. The medium was without (*top*) or with (*bottom*) 10 mM DTT. *E*, voltage-dependent open probability (P_{open}) of the mutant channel in presence of 10 mM DTT; $n = 4–6$. *Error bars*, S.D.

trol gating of the channel. The sequence of the MPV17 protein contains three predicted phosphorylation sites (Thr-53, Thr-80, and Ser-170; see Fig. 1*B*), and mutations in all of them were found to cause MDDS. We introduced a phosphomimicking mutation (p.T80D) into one of these sites, the closest to the predicted selectivity filter. The p.T80A variant mimicking a constitutively dephosphorylated protein was also generated. Like the wild-type MPV17 protein, both mutant variants formed homotrimers (data not shown).

The analyses of the channel properties using MCR (Fig. 8, *A* and *B*) and SCA (Fig. 8*C*) revealed insertion into an artificial membrane of two (low and high conductance) forms of the p.T80D channel. In contrast, high conductance was only registered with the p.T80A protein (Fig. 8*B*, *bottom*). This "high" conductance was nearly identical for both mutants and for the wild-type channel (compare Figs. 8 (*A–C*) and 2*D*, respectively). Importantly, the high conductance form of the MPV17 p.T80D protein was highly prone to closing even at low membrane potentials and with no addition of DTT, although this closing was mainly incomplete (Fig. 8. *D* and *E*). The residual conductance may reflect transformation of the channel from a fully open conformation to the subconductance state 4, as observed for the wild-type channel at high membrane potentials (see Fig. 4). Resistance toward voltage-dependent closing (Fig. 8, *D* and *F*) and low slope conductance ($\Lambda = 0.40 \pm 0.12$ nanosiemens, $n = 6$ (symmetrical 1.0 M KCl; Fig. 8*G*)) are in favor of this prediction.

Further analysis of the p.T80D channel revealed some shift in the ion selectivity (P_{K+}/P_{Cl-} ratio ~2.1; Fig. 9, *A* and *B*) relative to the wild-type control (see Fig. 3*D* for comparison). This is surprising if one considers localization of the phosphorylation site on the verge of the channel's pore (see Fig. 1*B* and "Discussion"). However, decreased cation selectivity of the channel after phosphorylation may be due to the conformational behavior of positively charged lysine residues (Lys-82, -87, and -88), which are situated just between the site of phosphorylation (Thr-80) and the amino acid (Asp-92) responsible for ion selectivity (see Fig. 1*B*). Likewise, no difference in ion selectivity was registered between the fully open mutant channel and its low conductance state (Fig. 9*B*).

Next, we tested whether redox conditions influence the channel properties of the MPV17 p.T80D protein. We found

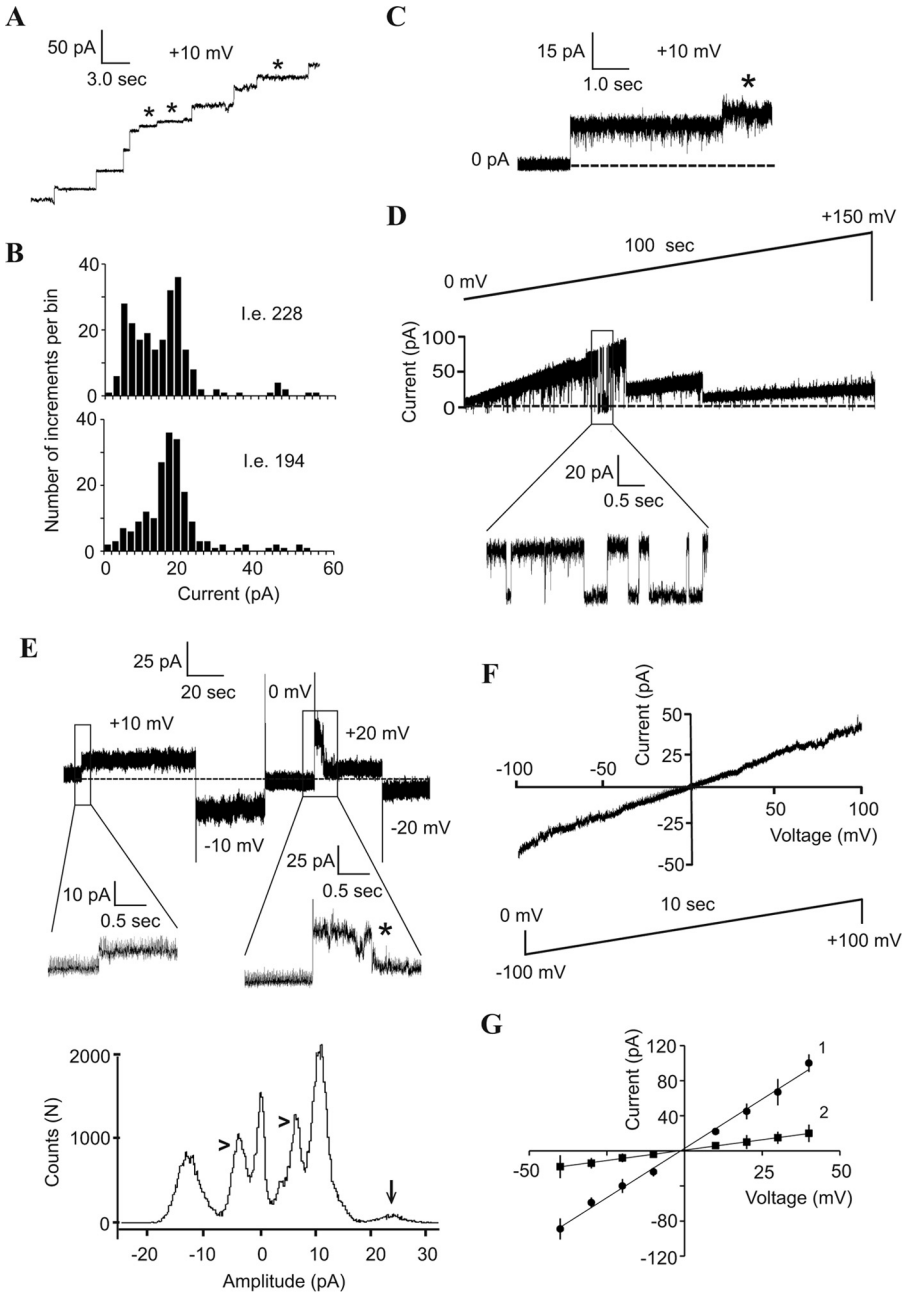

FIGURE 8. **Electrophysiological analyses of MPV17 protein carrying mutations p.T80D or p.T80A.** *A*, MCR of the p.T80D mutant channel. The low conductance insertions are marked by *asterisks*. Electrolyte (*A*, *C*, and *D–F*) was symmetrical 1.0 M KCl, pH 7.2, containing no DTT. *B*, histogram of the frequency of insertion events relative to their conductance. Bin size was 2 pA. *Top*, p.T80D channel; *bottom*, p.T80A channel. *C*, SCA recording of insertion of the two p.T80D channels. The low conductance insertion is marked by an *asterisk*. *D*, closing of a single p.T80D channel at positive voltages. The *bottom trace* represents time scale-expanded recording of the *top trace*. Note that closing of the channel is not complete (see also *E*). *E*, *top*, closing of p.T80D channel at low voltage. The *bottom traces* represent time scale-expanded recordings of the *top trace* showing insertion (*left trace*) and closing (*right trace*) events. The closing event is marked by an *asterisk*. *Bottom*, amplitude histogram derived from the recording shown at the *top*. The low conductance state registered after closing of the channel at +20 mV is marked by *arrowheads*. *Arrow*, counts registered at +20 mV for the channel at the fully open state. *F*, current-voltage dependence of the p.T80D channel at low conductance state that persisted after partial closing of the channel's pore (see *D* and *E*). *G*, current-voltage relationships of a mutant channel at the fully open (*1*) and the low conductance (*2*) states; $n = 5–7$. *Error bars*, S.D.

that pretreatment of the p.T80D protein with 0.2 mM H_2O_2 did not abolish the channel-forming activity at a wide range of membrane potentials (Fig. 9*C*), although it conferred some resistance to voltage-dependent closing (Fig. 9, *C* and *D*). In contrast, at reducing conditions (10 mM DTT), the mutant channel showed only traces of activity at membrane potentials equal to or below ±10 mV (Fig. 9*E*), indicating that the protein is inserted into the lipid bilayer. All further attempts to detect any activity of the mutant protein under reducing conditions and at membrane potentials above ±10 mV were without success, confirming that the channel is very voltage-sensitive.

The MPV17 p.T80A mutant mimicking the dephosphorylated protein showed features similar to the wild-type channel. The mutation did not affect the gating behavior of the channel (Fig. 9, *F* and *G*). Under reducing conditions, the channel showed closing, sometimes incomplete, with the appearance of

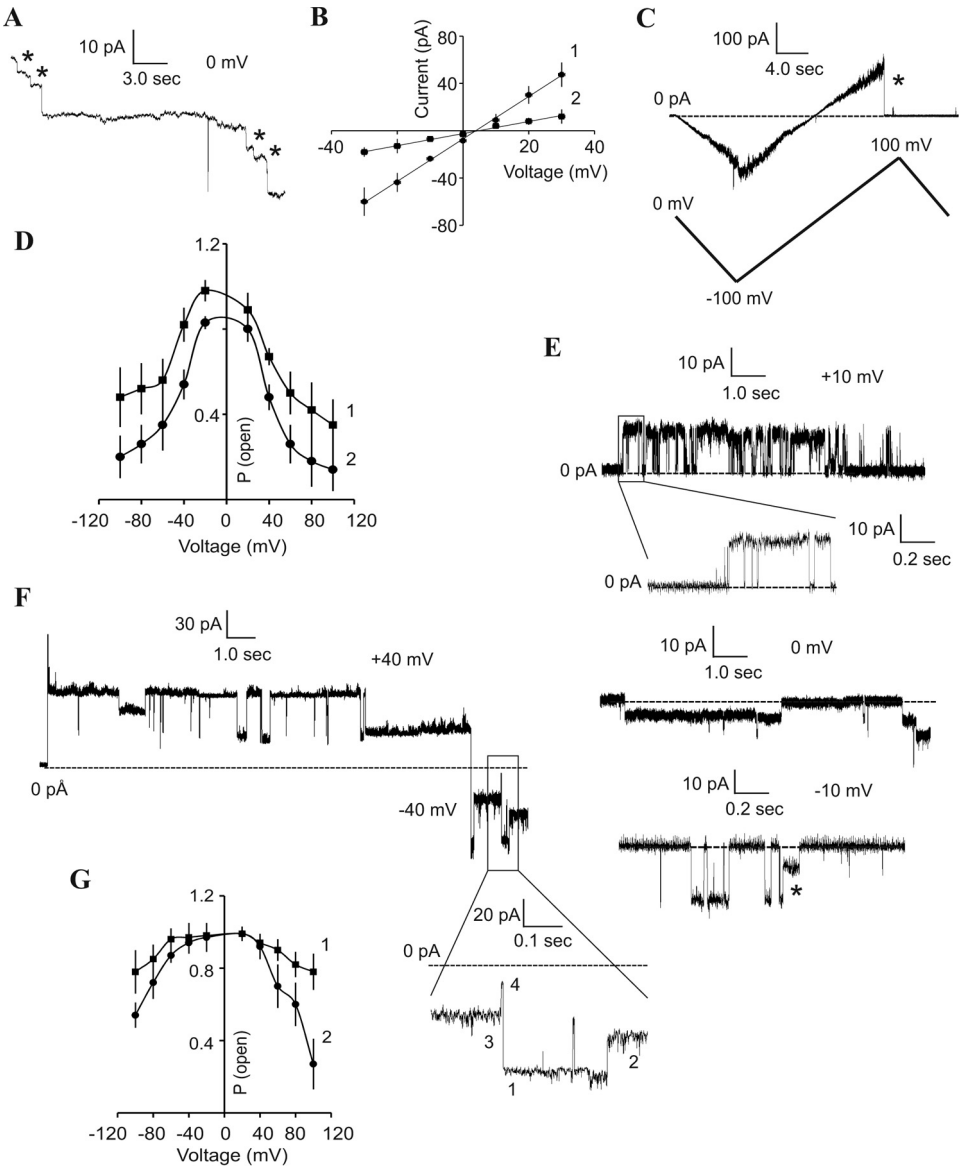

FIGURE 9. **Electrophysiological analysis of MPV17 protein with mutation p.T80D or p.T80A at different redox conditions.** *A*, MCR showing insertion of the p.T80D channels at fully open and low conductance (marked by *asterisks*) states. Electrolyte conditions (*A* and *B*) were asymmetric: 1.0 M KCl *trans*/0.5 M KCl *cis*, pH 7.2, with no addition of DTT. *B*, current-voltage dependence of the p.T80D channel at fully open (*1*) and low conductance (*2*) states. Note that ion selectivity of the channel is the same at both states. *C*, current trace of the p.T80D channel pretreated with 0.2 mM H_2O_2 in response to the indicated voltage ramp protocol. Electrolyte (*C* and *D*) was symmetrical 1.0 M KCl, pH 7.2, containing no DTT. Note the complete closing (marked by an *asterisk*) of the channel. *D*, voltage-dependent open probability (P_{open}) of p.T80D channel pretreated (*1*) or not treated (*2*) with H_2O_2 (0.2 mM) ($n = 3–6$). *E*, current traces of the single p.T80D channel at the indicated voltages. Electrolyte conditions were symmetric (1.0 M KCl, pH 7.2) with the exception of conditions at zero holding potential (1.0 M KCl *trans*/0.5 M KCl *cis*, pH 7.2). All samples contained 10 mM DTT. The *bottom trace* under recording at +10 mV shows an insertion event at higher time scale resolution. The subconductance state visible during recording at −10 mV is marked by an *asterisk*. *F*, recording of the single p.T80A channel at ±40 mV. Electrolyte was symmetrical 1.0 M KCl containing 10 mM DTT and buffered with 10 mM Tris-Cl, pH 7.2. The *bottom trace* represents time scale-expanded recording of the *top trace*. Note the partial closing of the channel with the appearance of four subconductance states (*numbered* at the *bottom trace*). *G*, voltage-dependent open probability (P_{open}) of p.T80A channel ($n = 4–6$). Electrolyte was symmetrical 1.0 M KCl, pH 7.2, without DTT (*1*) or containing 10 mM DTT (*2*). *Error bars*, S.D.

four subconductance states (Fig. 9*F*) or one-step complete closing (data not shown).

Together, these data support the view that phosphorylation of the MPV17 channel at Thr-80 may influence its voltage-dependent gating under oxidizing/reducing conditions. As a consequence, phosphorylation of MPV17, perhaps in more than one site, would lead to a complete closing of the channel, in particular under reducing conditions, even at near zero membrane potentials.

We further noticed that the MDDS-causing point mutation p.P98L is in proximity to the selectivity filter (Fig. 1*A*). This is remarkable because the conserved proline may form a helical turn important for gating of the channel. Substitution of proline by leucine did not abolish the channel-forming activity or affect the conductance of the channel (Fig. 10, *A* and *B*). The channel was prone to closing under reducing conditions (Fig. 10*C*); however, an incomplete closing of the channel was frequently observed (Fig. 10, *A* and *B*), which was in disagreement with observations on the

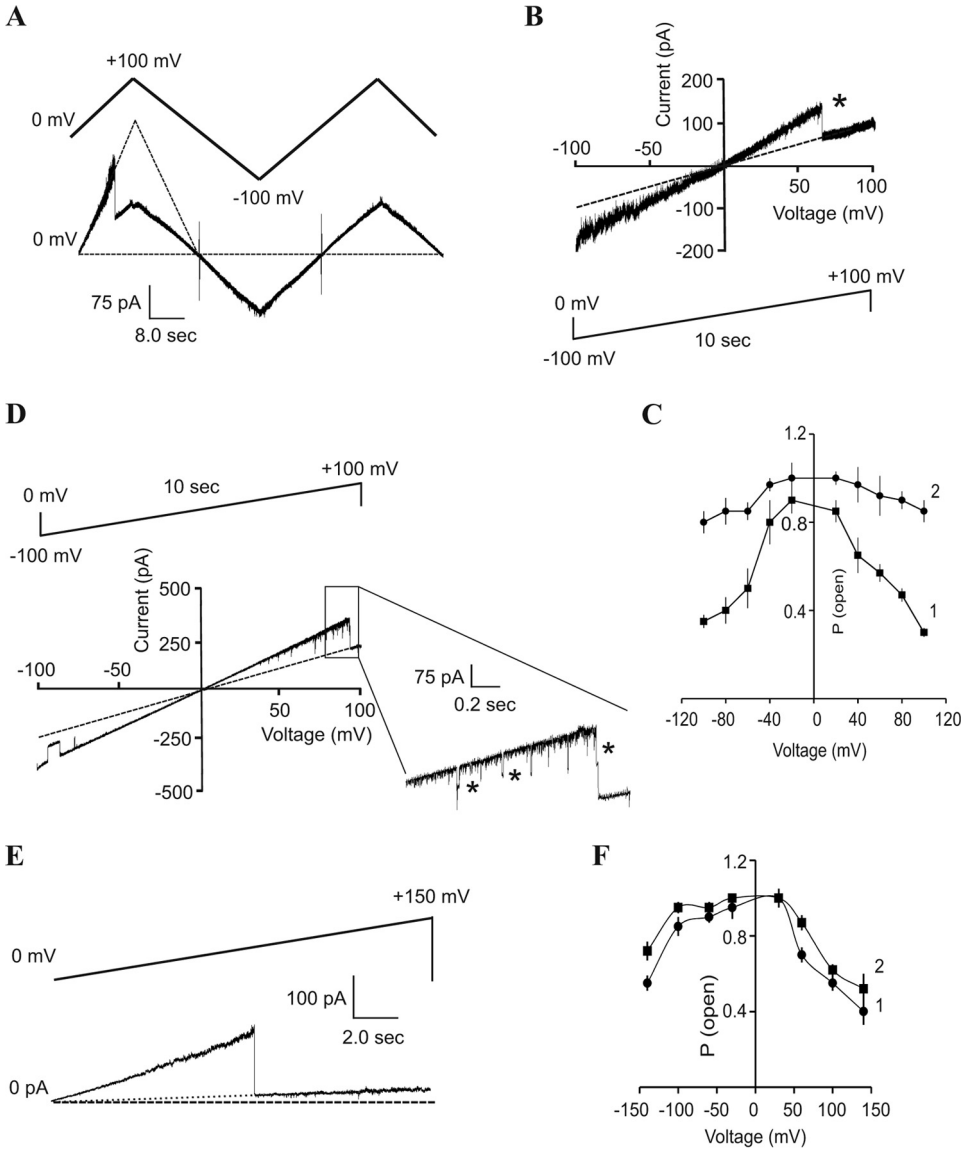

FIGURE 10. **SCA of MPV17 protein with mutations p.P98L or p.C99A.** *A*, current trace of the p.P98L channel in response to the indicated voltage ramp protocol. Electrolyte (*A* and *B*) was symmetrical 1.0 M KCl, pH 7.2, containing 10 mM DTT. Note the only partial closing (marked by *asterisks* in *A* and *B*) of the channel. *B*, current-voltage dependence of the p.P98L channel. *C*, voltage-dependent open probability (P_{open}) of the p.P98L channel registered in the presence (*1*) or absence (*2*) of 10 mM DTT. *D*, current-voltage dependence of two p.C99A channels according to the indicated voltage ramp protocol. The *bottom trace* represents a time scale-expanded recording of the *top trace* showing the appearance of subconductance state (marked by *asterisks*) during closing of one of the channels. Electrolyte (*D* and *E*) was symmetrical 1.0 M KCl, pH 7.2, containing no DTT. *E*, current trace of the single p.C99A channel in response to the indicated voltage ramp protocol. Protein sample was pretreated with 0.2 mM H_2O_2. *F*, voltage-dependent open probability (P_{open}) of the p.C99A channel. Electrolyte was symmetrical 1.0 M KCl, pH 7.2, without DTT. Protein samples were not treated (*1*) or were pretreated (*2*) with 0.2 mM H_2O_2. *Error bars*, S.D.

wild-type protein. This leads to the suggestion that Pro-98 might be required for tight locking of the channel's pore.

Cysteine 99 is the cysteine residue closest to the selectivity filter, and we expected that mutation of this amino acid might somehow affect redox regulation of the gating of MPV17 channel. The C99A mutant channel was active and showed conductance as well as gating properties at standard (no DTT) or reducing (10 mM DTT) conditions similar to that of the wild-type protein (Fig. 10*D*) (data not shown). However, pretreatment with 0.2 mM H_2O_2 did not prevent closing of the mutant channel at extreme holding potentials (Fig. 10, *E* and *F*), which is in contrast with properties of the wild-type channel (see Figs. 3*F* and 5 (*A*–*C*) for a comparison). This may indicate that cysteine 99 is oxidized only when harsh oxidative treatments are applied, and this amino acid does not affect the channel's gating at reducing conditions.

Together, our electrophysiological experiments showed that gating of the recombinant MPV17 channel is under control of different factors, such as membrane potential, pH, redox state, and apparently protein phosphorylation. Importantly, as is obvious from our data, closing of the channel is prevented under conditions deleterious for mitochondria. This led to the hypothesis that a transient opening of the channel may be beneficial for mitochondrial homeostasis. Indeed, opening of the non-selective channel would decrease $\Delta\psi_m$ and, as a result, prevent excessive formation of ROS (18, 32). Therefore, one of the MPV17 channel

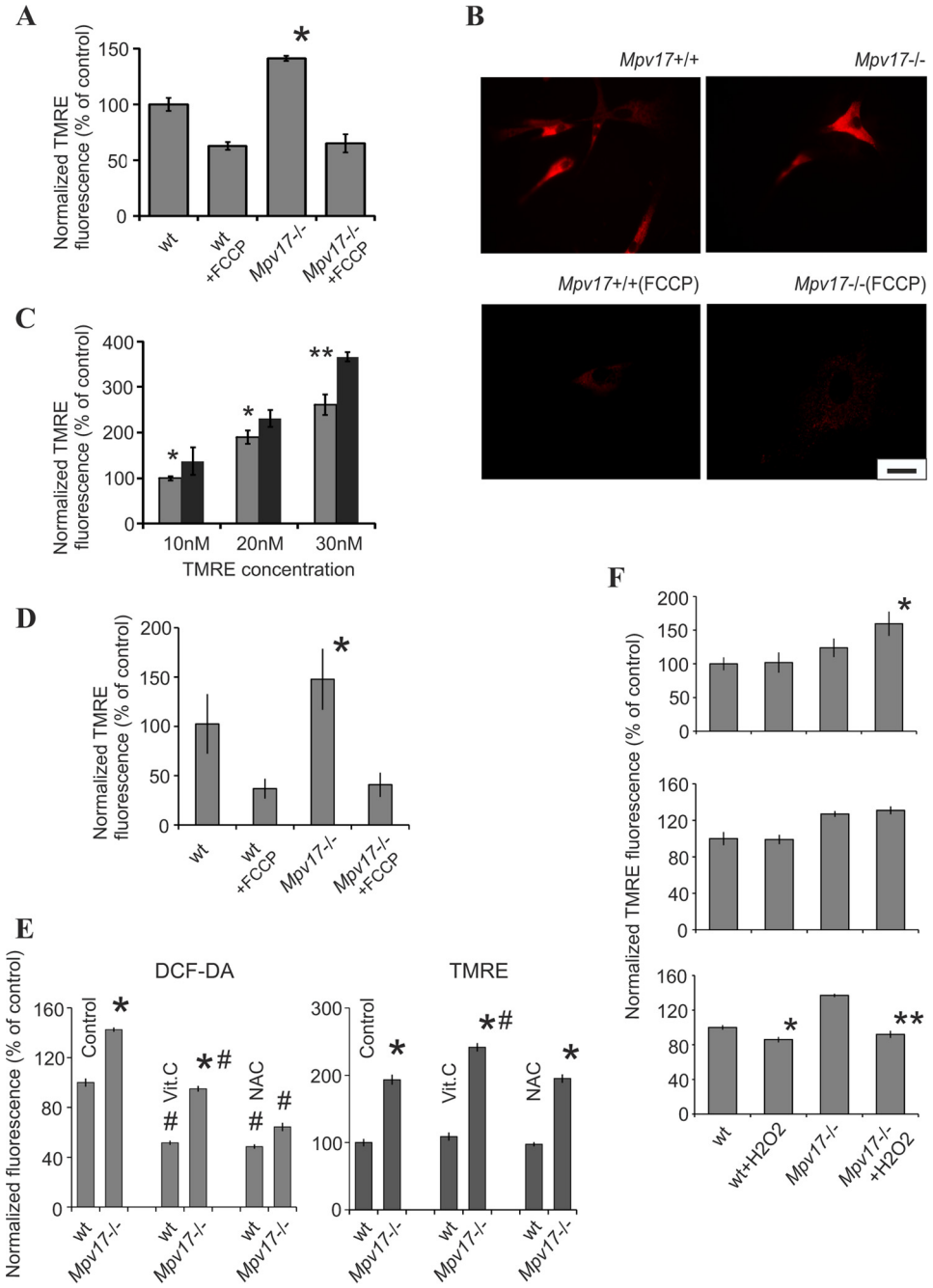

FIGURE 11. **Analysis of mitochondrial membrane potential and ROS formation in embryonic fibroblasts.** *A*, average TMRE fluorescence values of fibroblasts from wild-type and *Mpv17*$^{-/-}$ mice. Fluorescence intensity (*A*, *C*, *E*, and *F*) was detected by plate reading. *, $p < 0.001$; $n = 6$. 30 nM TMRE and 20 μM FCCP were used. *B*, live cell fluorescence microscopy of embryonic fibroblasts incubated with 30 nM TMRE. Note the low TMRE fluorescence of cells treated with 20 μM FCCP. *Scale bar*, 20 μM. *C*, dependence of the fluorescence values on TMRE concentration. *Light* and *dark bars*, results from wild-type and *Mpv17*$^{-/-}$ fibroblasts, respectively. *, $p < 0.05$; **, $p < 0.01$; $n = 4$. *D*, estimation of $\Delta\psi_m$ using digital image analysis (see "Experimental Procedures" for details). See the legend to Fig. 11*A* for the conditions used. *, $p < 0.05$; $n = 4$. *E*, average DCF-DA and TMRE fluorescence values in fibroblasts from wild-type and *Mpv17*$^{-/-}$ mice; effect of antioxidants: vitamin C (*Vit.C*; 100 μM) and *N*-acetyl-L-cysteine (*NAC*; 10 mM). Fibroblasts from the same stocks were used for all measurements. Note the increase in the level of DCF-DA fluorescence in *Mpv17*$^{-/-}$ fibroblasts, indicating excessive ROS production. Formation of ROS was severely suppressed by antioxidants (*left*). However, the antioxidants did not strongly affect the levels of $\Delta\psi_m$ (*right*). *, $p < 0.001$ (wild-type *versus* *Mpv17*$^{-/-}$ fibroblasts); #, $p < 0.001$ (control *versus* antioxidant-treated samples); $n = 4$. 30 nM TMRE and 10 μM DCF-DA were used. *F*, effect of H_2O_2 on $\Delta\psi_m$ of embryonic fibroblasts. The fluorescence was detected 4 h after a single injection of 50 μM H_2O_2 (*top*) or 48 h after injection of 200 μM H_2O_2 (*middle*). For chronic treatment of fibroblasts, 200 μM H_2O_2 was injected three times, every 5th day in a row and fluorescence measurements were conducted 48 h after the last injection (*bottom*). Cells immortalized after passage 5 were used. *, $p < 0.05$; **, $p < 0.01$; $n = 6$. *Error bars*, S.D.

functions may be conditional modulation of $\Delta\psi_m$. To verify this, we analyzed $\Delta\psi_m$ and ROS levels in embryonic fibroblasts from wild-type and Mpv17 knock-out mice (Fig. 11) by detecting TMRE (22) and DCF-DA (24, 25) fluorescence, respectively.

Accumulation of TMRE in mitochondria is a $\Delta\psi_m$-dependent process, and DCF-DA is considered to detect ROS that induce a broad set of oxidizing reactions during oxidative stress (25). The increase in TMRE fluorescence in mitochondria as a

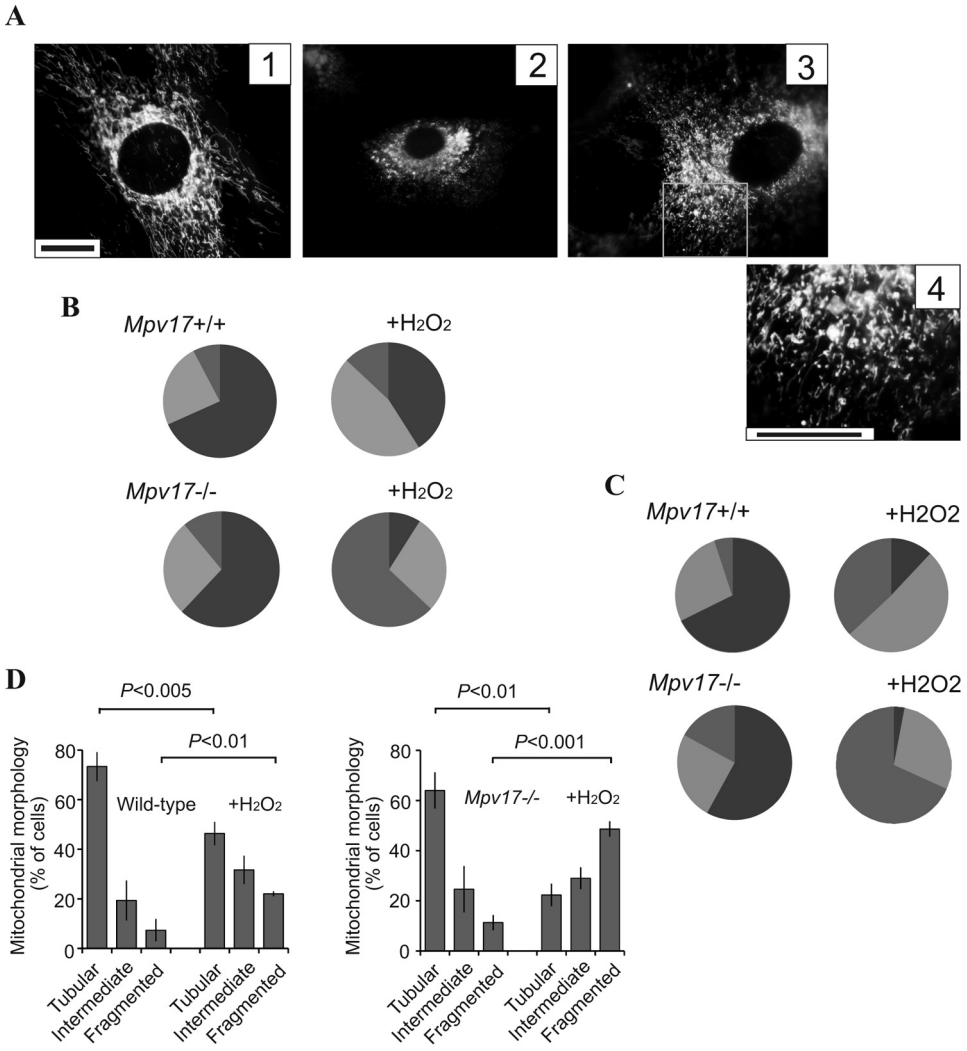

FIGURE 12. **Effect of H_2O_2 treatment on morphology of mitochondria.** *A*, representative images of fibroblasts with tubular (*1*) or completely (*2*) or partially (*3*) fragmented mitochondria. A higher magnification image of the *boxed area* in *3* is also shown (*4*). The cells were stained with 200 nM TMRE; *scale bar*, 20 μM. *B* and *C*, quantitative estimation of the effects of single (*B*) and chronic (*C*) H_2O_2 treatment (200 μM) on morphology of mitochondria (see legend to Fig. 11*F* for conditions of H_2O_2 treatment). The percentage of cells belonging to the corresponding morphological classification (see Fig. 12*A*) is shown: tubular (*dark gray*), partially fragmented (*light gray*), or completely fragmented (*gray*) mitochondria. 200 cells were scored for each group. Embryonic fibroblasts were immortalized after passage 5. *D*, semiquantitative analysis of mitochondrial morphology. The shape of mitochondria was detected according to Ref. 26 (see "Experimental Procedures" for details). Fibroblasts from wild-type and *Mpv17*$^{-/-}$ mice were used. Some samples (marked as $+H_2O_2$) were analyzed 4 h after single injection of H_2O_2 (50 μM). 120–140 cells were characterized for each group. *p* values are indicated; $n = 3$. *Error bars*, S.D.

$\Delta\psi_m$-dependent process was verified by pretreatment of cells with the protonophore uncoupler FCCP (Fig. 11, *A* and *B*). Our experiments demonstrated an elevated $\Delta\psi_m$ in intact *Mpv17*$^{-/-}$ fibroblasts compared with wild-type cells (Fig. 11, *A* and *C*). When conducting these measurements, we always verified that we used an equal number of cells and similar mass of mitochondria. The latter parameter was estimated using immunoblotting of mitochondrial "housekeeping" proteins (see below). Also, the $\Delta\psi_m$ increase in *Mpv17*$^{-/-}$ fibroblasts was not followed by changes in mitochondrial morphology (see Fig. 12 for details).

Finally, we verified our data using the digital image analysis procedure (see "Experimental Procedures"). The results of these experiments were very similar to those obtained by plate reading (Fig. 11, compare *A* and *D*). Importantly, hyperpolarization of mitochondria was accompanied by activation of ROS production, as revealed by the DCF-DA fluorescence (Fig. 11*E*, *left*). Our experiments with antioxidants (ascorbic acid and *N*-acetyl-L-cysteine) showing suppression of the DCF-DA fluorescence in embryonic fibroblasts is in accordance with this conclusion. Remarkably, the antioxidants did not affect $\Delta\psi_m$ in *Mpv17*$^{-/-}$ fibroblasts (Fig. 11*E*, *right*).

We then mimicked conditions of oxidative stress by treatment of cells with H_2O_2 at different concentrations. The reason for this was to reveal whether or not the Mpv17 channel is functional to prevent an excessive $\Delta\psi_m$ not only at physiological but also at stressful conditions. Low dose treatment with H_2O_2 did not affect the TMRE fluorescence in wild-type fibroblasts but significantly increased it in *Mpv17*$^{-/-}$ cells within 4 h (Fig. 11*F*, *top*). This effect of H_2O_2 on *Mpv17*$^{-/-}$ fibroblasts was temporary because the increased $\Delta\psi_m$ could no longer be detected after 48 h of the treatment (Fig. 11*F*, *middle*). These observations may reflect an appearance of the temporary hyperpolarization of mitochondria under oxidative stress (for a

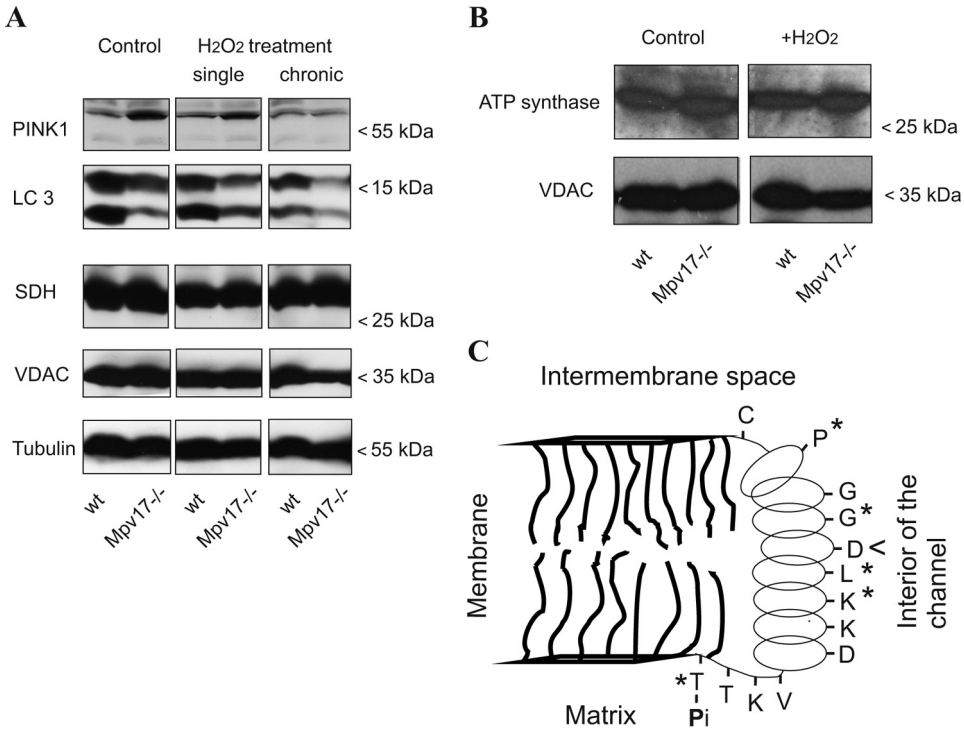

FIGURE 13. **Immunodetection of mitochondrial and cytosolic proteins.** *A*, PINK1 and LC3 proteins were detected in lysates of fibroblasts before (control) and after single or chronic H_2O_2 (200 μM) treatment (see the legend to Fig. 11*F* for details). Mitochondrial inner (*SDH*) and outer (*VDAC*) membrane proteins and cytosolic α-tubulin were analyzed as positive controls. *B*, immunodetection of the inner mitochondrial membrane protein ATP synthase subunit b (*ATP synthase*) in lysates of fibroblasts before (*Control*) and after ($+H_2O_2$) single H_2O_2 (200 μM) treatment of cells (see legend to Fig. 11*F* for details). *C*, hypothetical composition of the MPV17 channel interior. Only one α-helix (amino acids 80–99) of three identical amphipathic helices donated by each subunit of the homotrimeric MPV17 protein is shown. In addition to these helices, other parts of the protein molecule may participate in formation of the channel's pore. Amino acids forming the hydrophobic part of the helix (see Fig. 1, *B* and *C*) are not shown. The aspartic acid, Asp-92, responsible for ion selectivity of the channel is marked by an *arrowhead*. Locations of mutations leading to MDDS are marked by *asterisks*.

review, see Ref. 18) that is down-regulated by the Mpv17 channel in wild-type fibroblasts. Remarkably, chronic treatment with H_2O_2 over 5 days led to a drop of $\Delta\psi_m$ in both wild-type and *Mpv17*$^{-/-}$ cells. However, the rate of the decrease was much higher in the *Mpv17*$^{-/-}$ fibroblasts (35%) compared with the wild-type control (14%; Fig. 11*F*, *bottom*). Together, our data indicate that the Mpv17 channel is involved in the modulation of $\Delta\psi_m$ under normal conditions and under oxidative stress.

As established recently, the robust transmembrane potential is required not only for efficient oxidative phosphorylation but also for several other processes in mitochondria, such as morphogenesis (fission/fusion) (33, 34) and mitophagy (35, 36). Moreover, it seems that inhibition of fusion leading to the formation of fragmented mitochondria is a prerequisite of mitophagy (37). Therefore, modulation of membrane potential, fission, fusion, and mitophagy may be considered as a mitochondrial quality control axis (34, 37). Because the Mpv17 channel is involved in modulation of $\Delta\psi_m$ preventing overproduction of ROS (see above), the lack of this protein may compromise the quality control mechanisms in mitochondria. To verify this prediction, we inspected the shape of mitochondria in fibroblasts treated with 200 nM TMRE (Fig. 12*A*) and calculated cells containing tubular or fragmented particles (Fig. 12, *B–D*). To this end, we used two experimental approaches (see "Experimental Procedures") that showed similar results. Under standard conditions, the morphology of wild-type and Mpv17-deficient mitochondria was similar and represented mainly by tubular structures (Fig. 12, *A–D*). Single treatment of cells with H_2O_2 (200 μM) resulted in fragmentation of mitochondria that was more severe in *Mpv17*$^{-/-}$ fibroblasts (Fig. 12*B*), although these cells showed an elevated $\Delta\psi_m$ (see Fig. 11*F*, *middle*). After chronic treatment of wild-type fibroblasts with H_2O_2, a relatively large pool of cells with tubular mitochondria was still detected (Fig. 12*C*). In contrast, chronic H_2O_2 treatment led to almost total collapse of the tubular mitochondrial network in *Mpv17*$^{-/-}$ fibroblasts and to the predominant presence of completely fragmented mitochondria in these cells (Fig. 12*C*). Next, we compared our results on the morphology of mitochondria with those reported by others (26) using the same quantification procedure (see "Experimental Procedures" for details) but different reagents to visualize shape of the particles. In these experiments, we treated fibroblasts with H_2O_2 at low concentration (50 μM). After incubation for 4 h, we observed an intensive fragmentation of mitochondria (Fig. 12*D*, *left*). This was in accordance with results that have been obtained previously (26). The formation of fragmented mitochondria was more evident in *Mpv17*$^{-/-}$ fibroblasts when compared with wild-type cells (Fig. 12*D*, *right*).

The PINK1 protein is a key component of the PINK1/Parkin-dependent mitophagy machinery that is under regulatory control of $\Delta\psi_m$ (35, 36, 38). Immunodetection of PINK1 (Fig. 13*A*) showed that the amount of the unprocessed form of this protein (molecular mass 63 kDa) is higher in *Mpv17*$^{-/-}$ fibroblasts

when compared with wild-type cells. The same results were obtained after a single treatment of cells with H_2O_2. In contrast, chronic oxidative stress resulted in a significant decrease in the amount of $PINK1_{63}$ protein in *Mpv17*$^{-/-}$ cells. We also registered a decrease in the content of the autophagy-related LC3B protein in *Mpv17*$^{-/-}$ fibroblasts relative to the wild-type control. The changes in the content of $PINK1_{63}$ and LC3B proteins were specific because the amounts of the mitochondrial marker proteins succinate dehydrogenase and voltage-dependent anion channel as well as cytosolic α-tubulin were similar in *Mpv17*$^{-/-}$ and wild-type fibroblasts. In addition, we analyzed the content of mitochondrial ATP synthase subunit b. We did not find any difference in the amount of this protein between Mpv17$^{-/-}$ and wild-type fibroblasts (Fig. 13*B*). Together, our data indicate that Mpv17 specifically contributes to mitochondrial morphology and mitophagy.

Discussion

Here we showed that the human inner mitochondrial membrane protein MPV17 is a non-selective channel with gating properties under the regulatory control of a combination of several factors reflecting mitochondrial conditions, such as membrane potential, redox state, pH, and, apparently, protein phosphorylation. Recently, the information about channel-forming activity of the yeast inner mitochondrial membrane protein Sym1 homologous to mammalian Mpv17 and Pxmp2 proteins was published (16). These data together with our observations (this work) indicate that both peroxisomal (Pxmp2 (11)) and mitochondrial (fungal Sym1 (16) as well as mouse Mpv17 (15) and human MPV17) members of the Pxmp2 protein family are in fact membrane channels. Indeed, our preliminary data showing that other members of this family (human recombinant MP-L and FKSG24 (MPV17L2) proteins) are all active as non-selective channels in an artificial membrane are in line with this prediction.

Interestingly, mitochondrial MP-L, also known as Mpv17l, directly interacts with Omi/HtrA2 to enable protease activity of this protein (13). The interaction prevents mitochondrial dysfunction by reducing mitochondrial oxidative stress and stabilizing membrane potential. Omi/HtrA2 deficiency causes damage and mutation of mtDNA (39). The enzyme is regulated by the Parkinson disease-associated kinase PINK1 (40). Also, Sym1 protein is a heat-induced gene product that is required for cell growth under extreme conditions caused by ROS overproduction (41). Likewise, MPV17L2 protein is associated with the mitochondrial ribosome, and when its expression is reduced, the translation in the mitochondria is impaired (14). Altogether, these observations suggest that members of the mitochondrial branch of the Pxmp2 protein family are implicated in the correction of mitochondrial homeostasis, especially when it experiences stressful pressure from environmental factors. As follows from our data, this correction may result from the modulation of $\Delta\psi_m$ and transmembrane re-equilibration of metabolites by means of transient opening of the channel's pore.

On the whole, our data are clear in that the human MPV17 has the properties of a non-selective channel. The isolated recombinant protein showed in an artificial membrane the pore-forming activity with at least four subconductance levels, the highest one being 2.2 nanosiemens in 1.0 M KCl. The channel is moderately cation-selective and, in a fully open conformation, forms a membrane pore with a diameter of 1.8 nm. The size of the pore is large enough to predict that the channel is filled with water and allows transmembrane transfer of nearly all mitochondrial solutes, including inorganic ions, different metabolites, and even ATP molecules (the estimated size of the hydrated ATP molecule is 1.85×0.45 nm (42)).

Remarkably, the basic properties of channels constituting the Pxmp2 protein family (mammalian Pxmp2 and MPV17 and yeast Sym1) are similar. All of them are cation-selective channels with a large pore size (1.4 and 1.6 nm for Pxmp2 and Sym1, respectively) (11, 16). Under standard redox conditions (without the addition of reducing agents), the channels are resistant to closing at moderate membrane potentials. However, at membrane potentials above $\pm 100-120$ mV, the closing of the channels (frequently with the appearance of several subconductance states) is registered. However, in contrast to the MPV17 channel, which is under strict regulatory control by redox conditions, the peroxisomal Pxmp2 channel does not show such behavior.[6] This is reasonably to be expected because, in contrast to Mpv17 and Sym1, the sequence of Pxmp2 contains no cysteine residues.

Interestingly, our results indicate that under certain conditions, the MPV17 channel accommodates conformations (subconductance levels) intermediate between fully open and completely closed states. This apparently would lead to a decrease in the radius of the channel's pore relative to the size in a fully open conformation. Thus, from the conductance data (42), the diameter of the partially closed channel's pore at conformational state 4 (the state with the lowest conductance registered; see "Results") can be estimated to be ~0.8 nm, which allows transfer of inorganic ions but heavily limits diffusion of metabolites.

After discovery of channel-forming activities in the inner mitochondrial membrane using patch clamp technique (43, 44), a large set of results about electrophysiological properties of putative mitochondrial channels has been collected (for a review, see Ref. 17). However, information about proteins responsible for these activities is frequently missing. In several instances, our electrophysiological data on the isolated MPV17 channel are reminiscent of results obtained on the inner mitochondrial membrane using patch-clamp measurements (45, 46). Indeed, conductance values for the MPV17 channel are in the same range as those detected by De Marchi *et al.* (46) in the mitochondrial inner membrane of humans, mice, and rats. The activity was highly sensitive to voltage that coincides with our data on gating of the MPV17 channel at reducing conditions. However, the activity was evidently selective to anions, which is in contrast to the ion selectivity of MPV17 and other Pxmp2 family channels. Nevertheless, it should be stressed that our study has been carried out using purified recombinant MPV17 protein reconstituted in an artificial membrane, whereas the patch clamp technique preserves the channel in its native envi-

[6] V. D. Antonenkov, unpublished results.

ronment. This may cause differences in the results obtained. For example, phosphorylation of MPV17 protein may affect ion selectivity of the channel (see "Results").

The conclusion that the MPV17 is a non-selective channel evidently conflicts with the requirement to keep the inner mitochondrial membrane close to solutes to sustain metabolic activity and membrane potential of the functional mitochondria (17, 47, 48). The analysis of the gating properties of MPV17 channel was instrumental to resolve this issue. Indeed, our results indicate that the channel is effectively closed under conditions that can be expected for normally functioning mitochondria: high membrane potential, high ATP/ADP ratio that apparently favors protein phosphorylation, and reducing environment. This implies that voltage-dependent gating of the channel is under control of at least two key parameters indicating the state of the mitochondrial homeostasis: ATP availability and redox conditions. These data led us to suggest that the channel may be involved in mitochondrial quality control required for the correction of mitochondrial homeostasis (17, 32, 49, 50), morphogenesis (33, 34), or removal of damaged mitochondria by PINK1/Parkin-dependent mitophagy (35, 36, 38).

By using point mutation analysis, we succeeded in the detection of at least one amino acid (Asp-92) responsible for ion selectivity of the channel. As a rule, such an amino acid is localized very near or right inside the narrowest and hence the functionally most important part of the channel, the so-called selectivity filter. Next, we used knowledge of the location of a selectivity filter to introduce point mutations in the nearby amino acids that presumably form the interior of the channel's pore (Figs. 1*B* and 13*C*), aiming to resolve the role of these amino acids in voltage-dependent gating of the channel.

Introduction of the phosphomimicking mutation p.T80D prevents the opening of the channel at reducing conditions even without application of any membrane potential. This suggests a strong link between phosphorylation of the MPV17 protein and regulation of the channel-forming activity. Whether or not phosphorylation events in two other predicted phosphorylation sites of the protein (see Figs. 1*B* and 13*C*) are required for proper gating of the channel remains to be established. Mutations in these phosphorylation sites are responsible for the development of human MDDS (2, 5).

It seems that under oxidative conditions, the protein phosphorylation does not completely prevent closing of the channel but instead leads to a reduction in diameter of the channel's pore. This partial closing of the channel may be physiologically relevant to prevent leakage of ATP and cofactors from the mitochondrial matrix but at the same time to allow a drop in $\Delta\psi_m$ mainly due to transmembrane equilibration of the proton and inorganic ion gradients. At normal physiological conditions, an excessive $\Delta\psi_m$ that is accompanied by high ROS production (*i.e.* oxidative conditions) may be formed due to high availability of the substrates for oxidative phosphorylation together with low demand for mitochondrial ATP in the cell (18, 32, 50). Therefore, it is reasonable to predict the existence of protective mechanisms preventing "overheating" of the metabolic machinery in healthy mitochondria.

An antioxidant protective function has recently been predicted for several selective (potassium and chloride) ion channels in the inner mitochondrial membrane (51, 52) as well as for some members of the mitochondrial carrier family, such as uncoupling proteins (53). Moreover, the physiological role of the permeability transition pore in modulating $\Delta\psi_m$ has recently been postulated (18). Interestingly, the gating behavior of the MPV17 channel correlates in several aspects with predicted properties of this pore, including regulation by $\Delta\psi_m$, redox conditions, and pH. Whether or not all of these channels and transporters are really involved in regulation of $\Delta\psi_m$ remains to be established. However, these observations clearly indicate the vital importance of a tight regulation of $\Delta\psi_m$ to sustain mitochondrial homeostasis. This is important because both excessive and low $\Delta\psi_m$ may lead to a burst in ROS production (18) and affect many functions that depend on the appropriate $\Delta\psi_m$, such as biogenesis and dynamics of mitochondria, calcium sequestration, mitophagy, and others. In this sense, one can expect that MPV17 and related mitochondrial channels (MP-L and MPV17L2) are in fact local sensors of $\Delta\psi_m$, combining this function with efforts to prevent stressful conditions related to ROS overproduction and other negative factors.

Our observation of elevated $\Delta\psi_m$ (this work) in combination with the data on increased production of ROS (our results; see also Refs. 5 and 7) in cells from *Mpv17*$^{-/-}$ mice helps in understanding the apparent protective role of the Mpv17 channel in mitochondria. Treatment of *Mpv17*$^{-/-}$ fibroblasts with antioxidants, as expected, decreased the formation of ROS in both wild-type and *Mpv17*$^{-/-}$ cells. However, this treatment did not normalize $\Delta\psi_m$ in the Mpv17-deleted cells. The latter finding suggests that activation of ROS formation is downstream of the $\Delta\psi_m$ changes. One can expect that transient opening of the channel may prevent overproduction of mitochondrial ROS triggered by high $\Delta\psi_m$ (18, 32, 50). Deleterious effects of ROS on mtDNA stability and function of OXPHOS are well known (49, 50) and may explain the relatively low levels of mtDNA and mitochondrial dysfunction registered in *Mpv17*$^{-/-}$ fibroblasts (see Introduction). However, this latter prediction requires further experimental confirmation.

Presumably, the site of phosphorylation (Thr-80) mutated in our experiments faces a matrix space that allows interaction with a currently unknown protein phosphokinase (or protein phosphatase) involved in sensing the mitochondrial content of ATP. Therefore, two other mutated amino acids (Pro-98 and Cys-99) that are on the site opposite to the selectivity filter (Asp-92) should face the intermembrane space (Fig. 13*C*). Amino acid Pro-98 may be important for proper accommodation of the α-helical protein structure that is involved in formation of the channel's pore. Indeed, our data showing that the complete closing of the channel carrying the p.P98L mutation is compromised (see "Results") are in favor of this suggestion. Next, the p.C99A mutation led to some minor changes in the gating properties of the channel. These changes may be caused by an ability of the Cys-99 amino acid to sense the redox conditions in the intermembrane space, which, as known, are more oxidative than in the matrix (54).

Mitochondria are morphologically dynamic organelles. Their shape depends on two opposite processes, fusion and division (33, 34). Mounting evidence has revealed that depolarization of mitochondria impairs fusion, leading to the forma-

tion of fragmented particles (34, 55, 56). Here we analyzed how modulation of $\Delta\psi_m$ may affect the relative amount of tubular and fragmented mitochondria in wild-type and *Mpv17*$^{-/-}$ fibroblasts. Unexpectedly, we did not find any delay in fragmentation of *Mpv17*$^{-/-}$ mitochondria under oxidative conditions, although these particles showed an elevated $\Delta\psi_m$ relative to wild-type control. Instead, treatment of *Mpv17*$^{-/-}$ fibroblasts with H_2O_2 resulted in formation of a highly fragmented population of mitochondria, suggesting an inhibitory effect of Mpv17 deficiency on mitochondrial fusion. These findings outline a potential link between function of the Mpv17 channel and mitochondrial dynamics as part of the mitochondrial quality control axis. How the Mpv17 deficiency triggers fragmentation of mitochondria is not yet clear. One can expect that these mechanisms may rely on the mitochondrial ROS overproduction in *Mpv17*$^{-/-}$ fibroblasts. Indeed, we registered an increase in the amount of fragmented mitochondria after H_2O_2 treatment not only in *Mpv17*$^{-/-}$ fibroblasts but also in wild-type cells. ROS-induced mitochondrial fragmentation was previously observed by others (26, 57–59). In contrast, several groups have reported an increase in tubulation of mitochondria in response to oxidative stress (60–62). Indeed, the link between an elevated $\Delta\psi_m$, an oxidative stress, and mitochondrial morphology requires further experimental analysis.

As is obvious from our data, the MPV17 channel is prone to be fully open under conditions characteristic for damaged mitochondria. Persistent opening of the channel should inevitably lead to a total collapse of membrane potential that is a prerequisite of PINK1/Parkin-dependent mitophagy (35, 36). It is reasonable to assume that sensing of mitochondrial conditions followed by complete and persistent opening of the MPV17 channel are interlinked processes aiming to determine the fate of deficient mitochondria: whether or not to delete them by mitophagy. An apparent involvement of the MPV17 channel in mitophagy is supported by observations from Mpv17-deficient mice (4, 6, 8). Thus, tissues of Mpv17 knockout mice contain aberrant mitochondria with low content of mtDNA and cytochromes (4, 8). This may be due to a defect in mitochondrial quality control and mitophagy that leads to gradual accumulation of damaged mitochondria in somatic tissues. This process is known as a key factor of premature aging (63, 64), the condition that is characteristic for *Mpv17*$^{-/-}$ mice (4, 8). In our pilot study, we analyzed the content of PINK1 protein in wild-type and *Mpv17*$^{-/-}$ fibroblasts under normal conditions and after treatment of cells with H_2O_2 (see Fig. 13*A*). Indeed, the results indicated that PINK1/Parkin-dependent mitophagy is affected due to deletion of the Mpv17 channel. However, the detailed mechanism of this process is still not clear and requires further investigation. Interestingly, it seems that in addition to mitophagy, also the non-selective autophagy is compromised in *Mpv17*$^{-/-}$ fibroblasts, as could be seen by detection of the LC3B protein, which is a key indicator of autophagy (65). This finding suggests that the lack of the MPV17 channel may not only have an impact on mitophagy but also affect mechanisms leading to cell death (including apoptosis) and tissue damage (66). These potentially vast fields in biology of mitochondria await comprehensive investigation that requires different experimental approaches, including analyses of stress factors like ischemic insults in MPV17-deficient mice.

Our *in vitro* data indicate that mutations in human MPV17 causing MDDS (p.P98L and Thr-80 phosphorylation site (1, 2)) may affect gating properties of the channel by increasing the probability of the open configuration under stressful conditions. This observation, although preliminary, gives a clue to understanding the gross differences in phenotype of MDDS patients and *Mpv17*$^{-/-}$ mice (1–9). Indeed, some point mutations in MPV17 may produce a "leaky" channel that is unable to preserve high $\Delta\psi_m$. This situation is opposite to what can be expected from Mpv17 deletion: the total lack of channel-forming activity and hence inability to reduce an excessive $\Delta\psi_m$. Curiously, under these conditions, one can expect some quite similar aberrations in mitochondria as well as phenotype alterations in different tissues because in both cases an activation of ROS formation is highly expected (18). These conclusions, however, require further experimental verification, including *in situ* detection of the effects of MPV17 pathological mutations on cellular levels of $\Delta\psi_m$ and ROS production.

In conclusion, our results revealed that the MPV17 protein is a non-selective channel with gating properties affected by $\Delta\psi_m$, redox state, pH, and other conditions. The predicted function of the channel is a modulation of the membrane potential to preserve homeostasis in mitochondria and to conduct quality control of these organelles.

Acknowledgments—We thank Leena Ollitervo and Remya R. Nair for technical assistance.

References

1. El-Hattab, A. W., Li, F. Y., Schmitt, E., Zhang, S., Craigen, W. J., and Wong, L. J. C. (2010) MPV17-associated hepatocerebral mitochondrial DNA depletion syndrome: new patients and novel mutations. *Mol. Genet. Metab.* **99,** 300–308
2. El-Hattab, A. W., Scaglia, F., Craigen, W. J., and Wong, L. J. C. (2012) MPV17-related hepatocerebral mitochondrial DNA depletion syndrome. in *GeneReviews* (Pagon, R. A., Bird, T. D., Dolan, C. R., Stephens, K., and Adam, M. P., eds) University of Washington, Seattle, WA
3. El-Hattab, A. W., and Scaglia, F. (2013) Mitochondrial DNA depletion syndromes: review and updates of genetic basis, manifestations, and therapeutic options. *Neurotherapeutics* **10,** 186–198
4. Spinazzola, A., Viscomi, C., Fernandez-Vizarra, E., Carrara, F., D'Adamo, P., Calvo, S., Marsano, R. M., Donnini, C., Weiher, H., Strisciuglio, P., Parini, R., Sarzi, E., Chan, A., DiMauro, S., Rötig, A., Gasparini, P., Ferrero, I., Mootha, V. K., Tiranti, V., and Zeviani, M. (2006) MPV17 encodes an inner mitochondrial membrane protein and is mutated in infantile hepatic mitochondrial DNA depletion. *Nat. Genet.* **38,** 570–575
5. Uusimaa, J., Evans, J., Smith, C., Butterworth, A., Craig, K., Ashley, N., Liao, C., Carver, J., Diot, A., Macleod, L., Hargreaves, I., Al-Hussaini, A., Faqeih, E., Asery, A., Al Balwi, M., Eyaid, W., Al-Sunaid, A., Kelly, D., van Mourik, I., Ball, S., Jarvis, J., Mulay, A., Hadzic, N., Samyn, M., Baker, A., Rahman, S., Stewart, H., Morris, A. A., Seller, A., Fratter, C., Taylor, R. W., and Poulton, J. (2014) Clinical, biochemical and molecular characterization of mitochondrial DNA depletion syndrome due to novel mutations in the MPV17 gene. *Eur. J. Hum. Genet.* **22,** 184–191
6. Weiher, H., Noda, T., Gray, D. A., Sharpe, A. H., and Jaenisch, R. (1990) Transgenic mouse model of kidney disease: insertional inactivation of ubiquitously expressed gene leads to nephrotic syndrome. *Cell* **62,** 425–434
7. Binder, C. J., Weiher, H., Exner, M., and Kerjaschki, D. (1999) Glomerular

overproduction of oxygen radicals in Mpv17 gene-inactivated mice causes podocyte foot process flattening and proteinuria: a model of steroid-resistant nephrosis sensitive to radical scavenger therapy. *Am. J. Pathol.* **154,** 1067–1075
8. Viscomi, C., Spinazzola, A., Maggioni, M., Fernandez-Vizarra, E., Massa, V., Pagano, C., Vettor, R., Mora, M., and Zeviani, M. (2009) Early-onset liver mtDNA depletion and late-onset proteinuric nephropathy in Mpv17 knockout mice. *Hum. Mol. Genet.* **18,** 12–26
9. Casalena, G., Krick, S., Daehn, I., Yu, L., Ju, W., Shi, S., Tsai, S. Y., D'Agati, V., Lindenmeyer, M., Cohen, C. D., Schlondorff, D., and Bottinger, E. P. (2014) Mpv17 in mitochondria protects podocytes against mitochondrial dysfunction and apoptosis *in vivo* and *in vitro*. *Am. J. Physiol. Renal Physiol.* **306,** F1372–F1380
10. Bottani, E., Giordano, C., Civiletto, G., Di Meo, I., Auricchio, A., Cinsani, E., Marchet, S., Lamperti, C., d'Amati, G., Viscomi, C., and Zeviani, M. (2014) AAV-mediated liver-specific MPV17 expression restores mtDNA levels and prevents diet-induced liver failure. *Mol. Ther.* **22,** 10–17
11. Rokka, A., Antonenkov, V. D., Soininen, R., Immonen, H. L., Pirilä, P., Bergmann, U., Sormunen, R. T., Weckström, M., Benz, R., and Hiltunen, J. K. (2009) Pxmp2 is a channel-forming protein in mammalian peroxisomal membrane. *PLoS One* **4,** e5090
12. Antonenkov, V. D., and Hiltunen, J. K. (2012) Transfer of metabolites across the peroxisomal membrane. *Biochim. Biophys. Acta* **1822,** 1374–1386
13. Krick, S., Shi, S., Ju, W., Faul, C., Tsai, S. Y., Mundel, P., and Böttinger, E. P. (2008) Mpv17l protects against mitochondrial oxidative stress and apoptosis by activation of Omi/HtrA2 protease. *Proc. Natl. Acad. Sci. U.S.A.* **105,** 14106–14111
14. Dalla Rosa, I., Durigon, R., Pearce, S. F., Rorbach, J., Hirst, E. M. A., Vidoni, S., Reyes, A., Brea-Calvo, G., Minczuk, M., Woellhaf, M. W., Herrmann, J. M., Huynen, M. A., Holt, I. J., and Spinazzola, A. (2014) MPV17L2 is required for ribosome assembly in mitochondria. *Nucleic Acids Res.* **42,** 8500–8515
15. Antonenkov, V. D., and Hiltunen, J. K. (2011) Recombinant Mpv17 is a channel-forming protein. *Abstracts of the 3rd EMBO Meetings B108, Vienna, September 10–13, 2011*, p. 115, European Molecular Biology Organization, Heidelberg, Germany
16. Reinhold, R., Krüger, V., Meinecke, M., Schulz, C., Schmidt, B., Grunau, S. D., Guiard, B., Wiedemann, N., van der Laan, M., Wagner, R., Rehling, P., and Dudek, J. (2012) The channel-forming Sym1 protein is transported by the TIM23 complex in a presequence-independent manner. *Mol. Cell Biol.* **32,** 5009–5021
17. Szabo, I., and Zoratti, M. (2014) Mitochondrial channels: ion fluxes and more. *Physiol. Rev.* **94,** 519–608
18. Zorov, D. B., Juhaszova, M., and Sollott, S. J. (2014) Mitochondrial reactive oxygen species (ROS) and ROS-induced ROS release. *Physiol. Rev.* **94,** 909–950
19. Künkele, K. P., Heins, S., Dembowski, M., Nargang, F. E., Benz, R., Thieffry, M., Walz, J., Lill, R., Nussberger, S., and Neupert, W. (1998) The preprotein translocation channel of the outer membrane of mitochondria. *Cell* **93,** 1009–1019
20. Gincel, D., Zaid, H., and Shoshan-Barmatz, V. (2001) Calcium binding and translocation by the voltage-dependent anion channel: a possible regulatory mechanism in mitochondrial function. *Biochem. J.* **358,** 147–155
21. Wirth, A., Jung, M., Bies, C., Frien, M., Tyedmers, J., Zimmermann, R., and Wagner, R. (2003) The Sec61p complex is a dynamic precursor activated channel. *Mol. Cell* **12,** 261–268
22. Perry, S. W., Norman, J. P., Barbieri, J., Brown, E. B., and Gelbard, H. A. (2011) Mitochondrial membrane potential probes and the proton gradient: a practical usage guide. *BioTechniques* **50,** 98–115
23. Marks, J. D., Boriboun, C., and Wang, J. (2005) Mitochondrial nitric oxide mediates decreased vulnerability of hippocampal neurons from immature animals to NMDA. *J. Neurosci.* **25,** 6561–6575
24. Hempel, S. L., Buettner, G. R., O'Malley, Y. Q., Wessels, D. A., and Flaherty, D. M. (1999) Dihydrofluorescein diacetate is superior for detecting intracellular oxidants. *Free Radic. Biol. Med.* **27,** 146–159
25. Görlach, A., and Kietzmann, T. (2007) Superoxide and derived reactive oxygen species in the regulation of hypoxia-inducible factors. *Methods Enzymol.* **435,** 421–446
26. Frank, M., Duvezin-Caubet, S., Koob, S., Occhipinti, A., Jagasia, R., Petcherski, A., Ruonala, M. O., Priault, M., Salin, B., and Reichert, A. S. (2012) Mitophagy is triggered by mild oxidative stress in a mitochondrial fission dependent manner. *Biochim. Biophys. Acta* **1823,** 2297–2310
27. Drin, G., and Antonny, B. (2010) Amphipathic helices and membrane curvature. *FEBS Lett.* **584,** 1840–1847
28. Matsuzaki, K. (1998) Magainins as paradigm for the mode of action of pore forming polypeptides. *Biochim. Biophys. Acta* **1376,** 391–400
29. Roux, B., Bernèche, S., Egwolf, B., Lev, B., Noskov, S. Y., Rowley, C. N., and Yu, H. (2011) Ion selectivity in channels and transporters. *J. Gen. Physiol.* **137,** 415–426
30. Dishon, M., Zohar, O., and Sivan, U. (2011) Effect of cation size and charge on the interaction between silica surfaces in 1:1, 2:1, and 3:1 aqueous electrolytes. *Langmuir* **27,** 12977–12984
31. Scorrano, L., Petronilli, V., and Bernardi, P. (1997) On the voltage dependence of the mitochondrial permeability pore. *J. Biol. Chem.* **272,** 12295–12299
32. Murphy, M. P. (2009) How mitochondria produce reactive oxygen species. *Biochem. J.* **417,** 1–13
33. Ehses, S., Raschke, I., Mancuso, G., Bernacchia, A., Geimer, S., Tondera, D., Martinou, J-C., Westermann, B., Rugarli, E. I., and Langer, T. (2009) Regulation of OPA processing and mitochondrial fusion by m-AAA protease isoenzymes and OMA1. *J. Cell Biol.* **187,** 1023–1036
34. Youle, R. J., and van der Bliek, A. M. (2012) Mitochondrial fission, fusion, and stress. *Science* **337,** 1062–1065
35. Narendra, D. P., Jin, S. M., Tanaka, A., Suen, D. F., Gautier, C. A., Shen, J., Cookson, M. R., and Youle, R. J. (2010) PINK1 is selectively stabilized on impaired mitochondria to activate parkin. *PLoS Biol.* **8,** e1000298
36. Vives-Bauza, C., Zhou, C., Huang, Y., Cui, M., de Vries, R. L., Kim, J., May, J., Tocilescu, M. A., Liu, W., Ko, H. S., Magrané, J., Moore, D. J., Dawson, V. L., Grailhe, R., Dawson, T. M., Li, C., Tieu, K., and Przedborski, S. (2010) PINK1-dependent reqruitment of parkin to mitochondria in mitophagy. *Proc. Natl. Acad. Sci. U.S.A.* **107,** 378–383
37. Twig, G., Hyde, B., and Shirihai, O. S. (2008) Mitochondrial fusion, fission and authphagy as a quality control axis: the bioenergetic view. *Biochim. Biophys. Acta* **1777,** 1092–1097
38. Fedorowicz, M. A., de Vries-Schneider, R. L., Rüb, C., Becker, D., Huang, Y., Zhou, C., Alessi Wolken, D. M., Voos, W., Liu, Y., and Przedborski, S. (2014) Cytosolic cleaved PINK1 represses parkin translocation to mitochondria and mitophagy. *EMBO Rep.* **15,** 86–93
39. Goo, H. G., Jung, M. K., Han, S. S., Rhim, H., and Kang, S. (2013) HtrA2/Omi deficiency causes damage and mutation of mitochondrial DNA. *Biochim. Biophys. Acta* **1833,** 1866–1875
40. Plun-Fevreau, H., Klupsch, K., Moisoi, N., Gandhi, S., Kjaer, S., Frith, D., Harvey, K., Deas, E., Harvey, R. J., McDonald, N., Wood, N. W., Martins, L. M., and Downward, J. (2007) The mitochondrial protease HtrA2 is regulated by Parkison's disease-associated kinase PINK1. *Nat. Cell Biol.* **9,** 1243–1252
41. Dallabona, C., Marsano, R. M., Arzuffi, P., Ghezzi, D., Mancini, P., Zeviani, M., Ferrero, I., and Donnini, C. (2010) Sym1, the yeast ortholog of the MPV17 human disease protein, is a stress-induced bioenergetic and morphogenetic mitochondrial modulator. *Hum. Mol. Genet.* **19,** 1098–1107
42. Bölter, B., Soll, J., Hill, K., Hemmler, R., and Wagner, R. (1999) A rectifying ATP-regulated solute channel in the chloroplastic outer envelope from pea. *EMBO J.* **18,** 5505–5516
43. Sorgato, M. C., Keller, B. U., and Stühmer, W. (1987) Patch-clamping of the inner mitochondrial membrane reveals a voltage-dependent ion channel. *Nature* **330,** 498–500
44. Petronilli, V., Szabò, I., and Zoratti, M. (1989) The inner mitochondrial membrane contains ion-conducting channels similar to those found in bacteria. *FEBS Lett.* **259,** 137–143
45. Moran, O., Sandri, G., Panfili, E., Stühmer, W., and Sorgato, M. C. (1990) Electrophysiological characterization of contact sites in brain mitochondria. *J. Biol. Chem.* **265,** 908–913
46. De Marchi, U., Szabò, I., Cereghetti, G. M., Hoxha, P., Craigen, W. J., and Zoratti, M. (2008) A maxi-chloride channel in the inner membrane of mammalian mitochondria. *Biochim. Biophys. Acta* **1777,** 1438–1448

47. Caldeira da Silva, C. C., Cerqueira, F. M., Barbosa, L. F., Medeiros, M. H., and Kowaltowski, A. J. (2008) Mild mitochondrial uncoupling in mice affects energy metabolism, redox balance and longevity. *Aging Cell* **7,** 552–560
48. Kadenbach, B., Ramzan, R., Wen, L., and Vogt, S. (2010) New extension of the Mitchell theory for oxidative phosphorylation in mitochondria of living organisms. *Biochim. Biophys. Acta* **1800,** 205–212
49. Balaban, R. S., Nemoto, S., and Finkel, T. (2005) Mitochondria, oxidants, and aging. *Cell* **120,** 483–495
50. Kowaltowski, A. J., de Souza-Pinto, N. C., Castilho, R. F., and Vercesi, A. E. (2009) Mitochondria and reactive oxygen species. *Free Radic. Biol. Med.* **47,** 333–343
51. Heinen, A., Aldakkak, M., Stowe, D. F., Rhodes, S. S., Riess, M. L., Varadarajan, S. G., and Camara, A. K. S. (2007) Reverse electron flow-induced ROS production is attenuated by activation of mitochondrial Ca^{2+}-sensitive K^+ channels. *Am. J. Physiol. Heart Circ. Physiol.* **293,** H1400–H1407
52. Edwards, J. C., and Kahl, C. R. (2010) Chloride channels of intracellular membranes. *FEBS Lett.* **584,** 2102–2111
53. Mailloux, R. J., and Harper, M. E. (2011) Uncoupling proteins and the control of mitochondrial reactive oxygen species production. *Free Radic. Biol. Med.* **51,** 1106–1115
54. Mailloux, R. J., Jin, X., and Willmore, W. G. (2014) Redox regulation of mitochondrial function with emphasis on cysteine oxidation reactions. *Redox Biol.* **2,** 123–139
55. Legros, F., Lombès, A., Frachon, P., and Rojo, M. (2002) Mitochondrial fusion in human cells is efficient, requires the inner membrane potential, and is mediated by mitofusins. *Mol. Biol. Cell* **13,** 4343–4354
56. Liesa, M., Shirihai, O. S. (2013) Mitochondrial dynamics in the regulation of nutrient utilization and energy expenditure. *Cell Metab.* **17,** 491–506
57. Jendrach, M., Mai, S., Pohl, S., Vöth, M., and Bereiter-Hahn, J. (2008) Short- and long-term alterations of mitochondrial morphology, dynamics and mtDNA after transient oxidative stress. *Mitochondrion* **8,** 293–304
58. Fan, X., Hussien, R., and Brooks, G. (2010) H_2O_2-induced mitochondrial fragmentation in C_2C_{12} myocytes. *Free Radic. Biol. Med.* **49,** 1646–1654
59. Watanabe, T., Saotome, M., Nobuhara, M., Sakamoto, A., Urushida, T., Katoh, H., Satoh, H., Funaki, M., and Hayashi, H. (2014) Roles of mitochondrial fragmentation and reactive oxygen species in mitochondrial dysfunction and myocardial insulin resistance. *Exp. Cell Res.* **323,** 314–325
60. Gomes, L. C., Di Benedetto, G., and Scorrano, L. (2011) During autophagy mitochondria elongate, are spared from degradation and sustain cell viability. *Nat. Cell Biol.* **13,** 589–598
61. Rambold, A. S., Kostelecky, B., Elia, N., and Lippincott-Schwartz, J. (2011) Tubular network formation protects mitochondria from autophagosomal degradation during nutrient starvation. *Proc. Natl. Acad. Sci. U.S.A.* **108,** 10190–10195
62. Shutt, T., Geoffrion, M., Milne, R., and McBride, H. M. (2012) The mitochondrial redox state is a core determinant of mitochondrial fusion. *EMBO Rep.* **13,** 909–915
63. Wanagat, J., Dai, D. F., and Rabinovitch, P. (2010) Mitochondrial oxidative stress and mammalian healthspan. *Mech. Ageing Dev.* **131,** 527–535
64. Green, D. R., Galluzzi, L., and Kroemer, G. (2011) Mitochondria and the autophagy-inflammation-cell death axis in organismal aging. *Science* **333,** 1109–1112
65. Tanida, I., Minematsu-Ikeguchi, N., Ueno, T., and Kominami, E. (2005) Lysosomal turnover, but not a cellular level, of endogenous LC3 is a marker for autophagy. *Autophagy* **1,** 84–91
66. Navarro-Yepes, J., Burns, M., Anandhan, A., Khalimonchuk, O., del Razo, L. M., Quintanilla-Vega, B., Pappa, A., Panayiotidis, M. I., Franco, R. (2014) Oxidative stress, redox signaling, and autophagy: cell death *versus* survival. *Antioxid. Redox Signal.* **21,** 66–85